

ALGORITHMS FOR ℓ_p -BASED SEMI-SUPERVISED LEARNING ON GRAPHS

MAURICIO FLORES RIOS, JEFF CALDER, GILAD LERMAN

Department of Mathematics, University of Minnesota

ABSTRACT. We develop fast algorithms for solving the variational and game-theoretic p -Laplace equations on weighted graphs for $p > 2$. The graph p -Laplacian for $p > 2$ has been proposed recently as a replacement for the standard ($p = 2$) graph Laplacian in semi-supervised learning problems with very few labels, where the minimizer of the graph Laplacian becomes degenerate. We present several efficient and scalable algorithms for both the variational and game-theoretic formulations, and present numerical results on synthetic data and on classification and regression problems that illustrate the effectiveness of the p -Laplacian for semi-supervised learning with few labels.

1. INTRODUCTION

Data science problems, such as regression and classification, are pervasive in today's world, and the size of datasets is growing rapidly. In the supervised setting, data needs to be labeled, requiring substantial effort (e.g. writing a transcript for speech recognition), or may require expert input (deciding whether a brain scan is healthy or not). In contrast, unlabeled data can often be acquired in large quantities with substantially less effort. Semi-supervised learning aims to harness the additional information present in unlabeled data to improve learning tasks. This can include geometric or topological properties of unlabeled data, which can provide valuable information about where to place decision boundaries, for instance. This can be contrasted with fully supervised algorithms, such as neural networks, that typically learn parametrized functions, require abundant labeled data, and do not make use of unlabeled data.

A common setting within semi-supervised learning is *graph-based* semi-supervised learning, which is concerned with propagating label information on graphs. Here, we are given an undirected weighted graph $G = (\mathcal{X}, \mathcal{W})$, where \mathcal{X} are the vertices and $\mathcal{W} = \{w_{xy}\}_{x,y \in \mathcal{X}}$ are nonnegative edge weights, which are chosen so that $w_{xy} \approx 1$ when x is similar to y , and $w_{xy} \approx 0$ when x and y are dissimilar. Each vertex x in the *observation set* $\mathcal{O} \subset \mathcal{X}$ is assigned a label $g(x)$, where $g : \mathcal{O} \rightarrow \mathbb{R}$. The task of graph-based semi-supervised learning is to extend the labels from the observation set \mathcal{O} to the rest of the graph $\mathcal{X} \setminus \mathcal{O}$ in some meaningful way. Since this is *a priori* an ill-posed problem (there are infinitely many solutions), one usually makes the semi-supervised *smoothness assumption*, which asks that the learned labeling function $u : \mathcal{X} \rightarrow \mathbb{R}$ should be smooth in dense regions of the graph [12]. The smoothness assumption is often enforced by defining a functional (or regularizer) $J(u)$ that measures the *smoothness* of a labeling $u : \mathcal{X} \rightarrow \mathbb{R}$, and then minimizing $J(u)$ subject to either hard label constraints $u(x) = g(x)$ for $x \in \mathcal{O}$, or a soft penalty constraint. In this paper, we are concerned with learning problems with very few labels and so the hard constraint is necessary. All the techniques we discuss extend directly with minor modifications to soft constraints.

One of the most widely used methods in semi-supervised learning is Laplacian regularization [54], which uses the smoothness functional

$$(1.1) \quad J_2(u) := \frac{1}{4} \sum_{x,y \in \mathcal{X}} w_{xy} (u(x) - u(y))^2.$$

E-mail address: mauricio.a.flores.math@gmail.com, jcalder@umn.edu, lerman@umn.edu.
Source Code: https://github.com/mauriciofloresML/Laplacian_Lp_Graph_SSL.git.

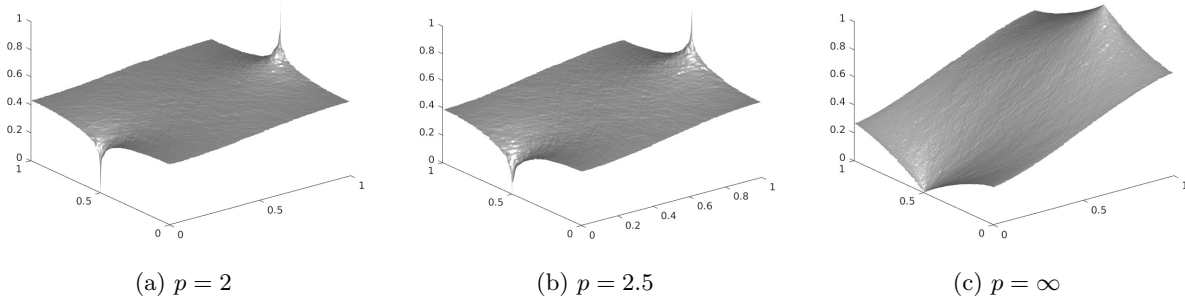


FIGURE 1. Numerical results for a toy learning problem with two labeled and 10^5 unlabeled data points on $[0, 1]^2$. For $p = 2$ the surface is nearly constant, with spikes near the labeled points, while as p becomes larger the surface becomes smoother.

Minimizing J_2 attempts to force similar data points in dense regions of the graph to have similar labels. Minimizers of J_2 are graph harmonic, and solve the graph 2-Laplace equation $\Delta_2^G u = 0$, where

$$(1.2) \quad \Delta_2^G u(x) := \sum_{y \in \mathcal{X}} w_{xy} (u(y) - u(x)).$$

In classification, the values of u are rounded to the nearest label. Laplacian regularization, and ideas based upon it, are very widely used in machine learning [3, 23, 24, 46, 48–51, 53], and have achieved great success. However, it has been noted first in [35] and later in [15], that Laplacian regularization becomes ill-posed (degenerate) in problems with very few labels. We say a graph-based learning problem is ill-posed in the limit of infinite unlabeled data and finite labeled data if the sequence of learned functions does not continuously attain the labeled (e.g., boundary) data in the continuum limit. In this case, the learned function becomes nearly constant on the whole graph, with sharp spikes near the labeled data. Thus, even with a hard constraint the labels are almost entirely ignored. See Figure 1a for a depiction of this degeneracy. In the continuum, this is merely reflecting the fact that the capacity of a point is zero in dimension $d \geq 2$ [29].

To address this issue, El Alaoui et al. [15] proposed a class of ℓ_p -based Laplacian regularizers, which use the smoothness functional

$$(1.3) \quad J_p(u) := \frac{1}{2p} \sum_{x,y \in \mathcal{X}} w_{xy} |u(x) - u(y)|^p.$$

Choosing $p > 2$ places a heavier penalty on large gradients $|u(x) - u(y)|$, which discourages the solution from developing sharp spikes. Minimizers of J_p satisfy the graph p -Laplace equation $\Delta_p^G u = 0$, where

$$(1.4) \quad \Delta_p^G u(x) := \sum_{y \in \mathcal{X}} w_{xy} |u(x) - u(y)|^{p-2} (u(y) - u(x)).$$

We call (1.4) the *variational graph p -Laplacian*. Figure 1 depicts ℓ_p regularization for different values of p . As p increases the learned function transitions more smoothly between labeled and unlabeled points. From a continuum perspective, the energy J_p is related to the p -Dirichlet energy $\int_{\Omega} |\nabla u|^p dx$, and the Sobolev embedding $W^{1,p}(\Omega) \hookrightarrow C^{0,1-d/p}(\Omega)$ allows isolated boundary points

when $p > d$, where d is the dimension.¹ Indeed, by Morrey's inequality [19] we have

$$(1.5) \quad |u(x) - u(y)| \leq C \left(\int_{\Omega} |\nabla u|^p dx \right)^{1/p} |x - y|^{1-d/p}$$

whenever $p > d$ and $|x - y| \leq \frac{1}{2} \text{dist}(x, \partial\Omega)$. Morrey's inequality implies that u is Hölder continuous, and prevents spikes from occurring as in Figure 1a. In particular, the continuum p -Dirichlet problem (see (1.10)) with constraints at isolated points is well-posed (e.g., admits a unique solution attaining the boundary data continuously) if and only if $p > d$.

The variational graph p -Laplacian (1.4) has appeared previously in machine learning [1, 5, 52], but was first suggested for problems with few labels in [15] with $p \geq d + 1$. Recently, it was rigorously proven that ℓ_p -based regularization is ill-posed (its minimizer is degenerate) for $p \leq d$, and well-posed for $p > d$ in the continuum limit of infinite unlabeled and finite labeled data [43]. This justifies the continuum heuristics described above. Thus, it is important to have efficient algorithms for solving $\Delta_p^G u = 0$ for large values of p . Since the model involves a large exponent p , it can become ill-conditioned numerically when p is large (see Section 3).

Formally sending $p \rightarrow \infty$ in (1.3) one obtains *Lipschitz learning* [27, 33], which corresponds to the smoothness functional

$$(1.6) \quad J_{\infty}(u) = \max_{x,y \in \mathcal{X}} w_{xy} |u(x) - u(y)|.$$

Minimizers of (1.6) are not unique and thus must be interpreted in an appropriate sense. In [27] the authors solve for the solution whose gradient is smallest in the lexicographical order, called the *lex-minimizer*, which is equivalent to the notion of *absolutely minimal* in the analysis community [4]. Lex-minimizers of (1.6) satisfy the graph ∞ -Laplace equation $\Delta_{\infty}^G u = 0$ where

$$(1.7) \quad \Delta_{\infty}^G u(x) := \min_{y \in \mathcal{X}} w_{xy} (u(y) - u(x)) + \max_{y \in \mathcal{X}} w_{xy} (u(y) - u(x)).$$

It was proved recently [6] that Lipschitz learning is well-posed with arbitrarily few labels. However, in the continuum the algorithm ignores the distribution of unlabeled data and loses some of the advantages of semi-supervised learning.

In order to combine the well-posedness of Lipschitz learning with the distributional sensitivity of Laplacian regularization, it is natural to augment the 2-Laplacian with a small ∞ -Laplace term and solve an equation of the form $\Delta_2^G u + \varepsilon \Delta_{\infty}^G u = 0$. To this end, we define the *game theoretic p -Laplacian* on the graph (we later clarify the name of this p -Laplacian)

$$(1.8) \quad \mathcal{L}_p^G u(x) = \frac{1}{d_x p} \Delta_2^G u(x) + \lambda \left(1 - \frac{2}{p}\right) \Delta_{\infty}^G u(x),$$

where $d_x = \sum_{y \in \mathcal{X}} w_{xy}$ is the degree of vertex x , and $\lambda > 0$ is a constant. For semi-supervised learning with the game-theoretic p -Laplacian we solve $\mathcal{L}_p^G u = 0$ subject to $u = g$ on \mathcal{O} (see Section 1.2 for precise definitions). Calder [7] proved the game theoretic p -Laplacian is well-posed with very few labels for $p > d$, and argued for the use of this formulation as an alternative regularization for semi-supervised learning on graphs. In the context of these results, λ is chosen (explicitly) depending on the kernel used to define the weights w_{xy} . For simplicity, we take $\lambda = 1$ in the rest of the paper. Compared to the variational p -Laplacian, the game-theoretic p -Laplacian appears better conditioned numerically when p is large, since it does not require computing large powers of p . Another main difference is that the game-theoretic p -Laplacian does not arise through an optimization problem, and so the methods for solving the equation are somewhat different. We note that the game-theoretic graph p -Laplacian (and similar models) have been used very recently for data clustering and learning problems [16–18, 22], though not in the context of very few labeled

¹Here, $\Omega \subset \mathbb{R}^d$ is an open, bounded domain, and $W^{1,p}(\Omega)$ is the Sobolev space of functions $u : \Omega \rightarrow \mathbb{R}$ such that $\int_{\Omega} u^p + |\nabla u|^p dx < \infty$.

data points. A related definition of the game-theoretic p -Laplacian on graphs was also studied in [34]. We also mention recent work [9, 42] that approaches the semi-supervised learning problem with few labels by re-weighting the graph so that the weights w_{xy} are large near labels.

Both the variational (1.4) and the game-theoretic (1.8) graph p -Laplace equations are consistent in the continuum with the p -Laplace equation

$$(1.9) \quad \Delta_p u := \operatorname{div}(|\nabla u|^{p-2} \nabla u) = 0.$$

The operator Δ_p is called the p -Laplacian, and solutions of (1.9) are called p -harmonic functions [31]. The p -Laplace equation arises as the necessary conditions (Euler-Lagrange equation) for the p -Dirichlet problem

$$(1.10) \quad \min_u \int_{\Omega} |\nabla u|^p dx.$$

Note that we can expand the p -Laplacian to obtain

$$\Delta_p u = |\nabla u|^{p-2} (\Delta u + (p-2) \Delta_{\infty} u),$$

where Δ_{∞} is the ∞ -Laplacian, given by

$$(1.11) \quad \Delta_{\infty} u := \frac{1}{|\nabla u|^2} \sum_{i,j=1}^d u_{x_i x_j} u_{x_i} u_{x_j}.$$

Thus, any solution of $\Delta_p u = 0$ also satisfies

$$(1.12) \quad \frac{1}{p} \Delta u + \left(1 - \frac{2}{p}\right) \Delta_{\infty} u = 0.$$

The right hand side is often called the *game-theoretic* or *homogeneous* p -Laplacian since it arises in two player stochastic tug-of-war games [30, 38]. This justifies the definition (1.8) of the game-theoretic graph p -Laplacian. We note that while the p -Laplace equation (1.9) is equivalent to the game theoretic version (1.12) at the continuum level, these are different formulations on the graph.

Given the recent interest in graph p -Laplacian models in machine learning, it is important to have efficient and scalable algorithms for real-world problems. There are relatively few works on fast algorithms for graph p -Laplacians. Kyng et al., [27] developed an efficient algorithm for Lipschitz learning ($p = \infty$). Their algorithm has a poor worst case complexity analysis (roughly quadratic complexity in the number of data points), but seems to run very fast—nearly linear time—in practice. Oberman [36] considers the game-theoretic formulation on regular grids in dimensions $d = 2, 3$, and developed a fast semi-implicit solution method, as well as gradient-descent methods. One contribution of this paper is an adaptation of Oberman’s semi-implicit method to the graph setting. Other works [16–18] use slow iterative methods, such as Jacobi iteration or gradient descent. It was suggested in [15] to use Newton’s method for the variational p -Laplacian, but the method was not investigated in any depth. The energy J_p is smooth and convex, but not strongly convex when $p > 2$. Other works, such as [27], suggest to use convex programming to solve the variational p -Laplacian.

In this paper, we develop and study a broad range of algorithms for solving the variational and game-theoretic graph p -Laplace equations, and identify the algorithms that are efficient and scalable in each setting. We conduct extensive numerical tests on the methods, first on synthetic data in low and high dimensions, and then on real data sets, including MNIST [28], Fashion MNIST [47], and real-world regression problems [26, 44]. In particular, we study classification problems with very few labels, and show that graph p -Laplacian learning with $p > 2$ is superior to Laplacian regularization. Furthermore, we show that the p -Laplace formulations become more accurate at classification when given access to more unlabeled data, which confirms the semi-supervised learning paradigm. We also demonstrate competitive accuracy and speed of some of the proposed methods, in particular,

of the semi-implicit method for the graph-theoretic p -Laplacian with $p > 2$. We give an outline of the paper below.

1.1. Outline. First, in Section 1.2 we set notation and clearly define each problem, and in Section 1.3 we give a brief summary of all method and their advantages and disadvantages, including recommendations for the user. In Section 2 we discuss two standard algorithms to solve the variational p -Laplace equation, followed by a primal dual approach, which eliminates the need to solve a linear system, or having to compute large powers of p . Numerical results for all three methods are provided in Section 3. In Section 4 we discuss two standard approaches to solving the game theoretic problem, and later two original algorithms. We present numerical results for the game-theoretic p -Laplace equation in Section 5. In Section 6 we present the results of simulations with real-world classification and regression problems with very few labels, and we conclude this work in Section 7. Our code is available for download at https://github.com/mauriciofloresML/Laplacian_Lp_Graph_SSL.git.

1.2. Definitions. Here, we give precise definitions of the variational and game-theoretic p -Laplacians on a graph. Let us recall that we are given an undirected weighted graph $G = (\mathcal{X}, \mathcal{W})$, where \mathcal{X} are the vertices and $\mathcal{W} = \{w_{xy}\}_{x,y \in \mathcal{X}}$ are nonnegative edge weights, a subset $\mathcal{O} \subset \mathcal{X}$ of labeled vertices, and labels $g : \mathcal{O} \rightarrow \mathbb{R}$. We denote the number of data points in \mathcal{O} by m , and the number of data points in $\mathcal{X} \setminus \mathcal{O}$ by n . We are interested in the setting where $n \gg m$, meaning that the amount of unlabeled data far exceeds labeled data. We will assume throughout the paper that the graph is connected, which is required to ensure uniqueness of solutions to the graph-based problems described below. Here, *connected* means that between any two vertices $x, y \in \mathcal{X}$, there is a path $x = x_1, x_2, \dots, x_k = y$ such that $w_{x_i x_{i+1}} > 0$ for each i .

The ℓ_p -based Laplacian regularized learning problem [15] is given by

$$(1.13) \quad \min_{u: \mathcal{X} \rightarrow \mathbb{R}} J_p(u) \quad \text{subject to } u(x) = g(x) \text{ for all } x \in \mathcal{O},$$

where we extend the definition of J_p to be

$$(1.14) \quad J_p(u) := \frac{1}{2p} \sum_{x,y \in \mathcal{X}} w_{xy} |u(x) - u(y)|^p + \sum_{x \in \mathcal{X}} f(x)u(x),$$

where f is a source function (more details below). The unique minimizer $u : \mathcal{X} \rightarrow \mathbb{R}$ of (1.13) satisfies the optimality conditions

$$(1.15) \quad \begin{cases} -\Delta_p^G u(x) = f(x) & \text{if } x \in \mathcal{X} \setminus \mathcal{O} \\ u(x) = g(x) & \text{if } x \in \mathcal{O}, \end{cases}$$

where Δ_p^G is defined in (1.4). While we most often are concerned with $f \equiv 0$ in practice, it is useful to formulate the problem in more generality, so that we can easily compute exact solutions by choosing $u(x)$ and computing $f(x)$ accordingly. We will refer to (1.13) as the **variational problem**, and to (1.15) as the **variational p -Laplace equation**.

The game-theoretic graph p -Laplacian regularized semi-supervised learning problem corresponds to solving

$$(1.16) \quad \begin{cases} -\mathcal{L}_p^G u(x) = f(x) & \text{if } x \in \mathcal{X} \setminus \mathcal{O} \\ u(x) = g(x) & \text{if } x \in \mathcal{O}, \end{cases}$$

where \mathcal{L}_p^G is the game-theoretic graph p -Laplacian defined in (1.8). We will refer to (1.16) as the **game-theoretic problem**. As before, we are concerned mainly with $f \equiv 0$. Note that the game-theoretic problem does not arise from a variational principle. The **Lipschitz learning problem** corresponds to the game-theoretic problem with $p = \infty$.

1.3. Summary of Methods. In this section we briefly outline the methods we have developed/studied, alongside their advantages and disadvantages.

1.3.1. *Methods for Variational Problem.* We consider three methods: IRLS, Newton and Primal Dual. IRLS is not useful, as it only converges when $p < 3$. Newton's method may handle large p powers with the use of homotopy. It requires solving a large and sparse system of equations at each iteration, but this is manageable with an iterative solver. Among its limitations, convergence is not guaranteed away from a solution, and roundoff errors can have some negative impact on accuracy. Finally, the Primal Dual method, unlike IRLS and Newton, does not require inverting a linear system at each iteration, and does not need to compute powers of p , which reduces the concern over roundoff errors, and is guaranteed to converge, but it converges with a very slow rate of $O(1/N)$. In practice, linear convergence may be achieved if the method is tuned appropriately, but doing so is challenging. Overall, Newton's method with homotopy is the best alternative.

1.3.2. *Methods for Game Theoretic Problem.* We discuss three methods: gradient descent, Newton-like, and semi-implicit. The gradient descent method converges with a slow linear rate, but is reliable and easy to implement. The Newton-like algorithm converges very quickly when near the solution, but may not converge at all far from it. This method can handle large p values with the use of homotopy. The semi-implicit method converges with a fast linear rate, and may handle large p values without any issues. For this method, we invert the same linear system at each iteration, and precompute a factorization which decreases the computational cost substantially. In most cases, the semi-implicit method is the best alternative for the game-theoretic formulation.

1.4. **Acknowledgements.** The authors gratefully acknowledge National Science Foundation grants 1713691, 1821266, 1830418, and a University of Minnesota Grant in Aid Award.

2. ALGORITHMS FOR VARIATIONAL PROBLEM

We first address computational algorithms for the variational p -Laplace equation (1.15). We consider an iteratively reweighted least squares solver (Section 2.1), Newton's method (Section 2.2), and a primal-dual approach (Section 2.3).

It is useful to first rewrite the function $J_p(u)$ using vector notation. Let $\mathcal{X} = \{x^1, \dots, x^{n+m}\} \subset \mathbb{R}^d$, where $\mathcal{O} = \{x^{n+1}, \dots, x^{n+m}\}$ is the observation set. We define $u_i = u(x^i)$ and set $\mathbf{u} = (u_1, \dots, u_n) \in \mathbb{R}^n$. Similarly, set $w_{ij} = w_{x_i x_j}$, $f_i = f(x^i)$, $g_i = g(x^{i+n})$, $\mathbf{f} = (f_1, \dots, f_n) \in \mathbb{R}^n$, and $\mathbf{g} = (g_1, \dots, g_m) \in \mathbb{R}^m$. Then, subject to the constraints given in 1.13, we can write

$$(2.1) \quad J_p(\mathbf{u}) = \frac{1}{p} \left(\sum_{i=1}^n \sum_{j=i+1}^n w_{ij} |u_i - u_j|^p + \sum_{i=1}^n \sum_{j=1}^m w_{i,j+n} |u_i - g_j|^p \right) + \sum_{i=1}^n f_i u_i.$$

2.1. **An Iteratively Reweighted Least Squares Solver.** We begin by writing the minimization of (2.1) as an Iteratively Reweighted Least Squares (IRLS) problem (see [11]). At each iteration k , we solve

$$(2.2) \quad \mathbf{u}^{k+1} = \arg \min_{\mathbf{u} \in \mathbb{R}^n} \left\{ \frac{1}{2} \left(\sum_{i=1}^n \sum_{j=i+1}^n w_{ij}^k |u_i - u_j|^2 + \sum_{i=1}^n \sum_{j=1}^m w_{i,j+n}^k |u_i - g_j|^2 \right) + \sum_{i=1}^n f_i u_i^k \right\},$$

where $w_{ij}^k = w_{ij} |u_i^k - u_j^k|^{p-2}$ and $w_{i,j+n}^k = w_{i,j+n} |u_i^k - g_j|^{p-2}$. Differentiating (2.2) we find that \mathbf{u}^{k+1} satisfies

$$(2.3) \quad \sum_{j=1}^m w_{i,j+n}^k u_i^{k+1} - \sum_{j=1}^n w_{ij}^k (u_j^{k+1} - u_i^{k+1}) = \sum_{j=1}^m w_{i,j+n}^k g_j + f_i,$$

for all $i \in \{1, \dots, n\}$. Define $a_{ij}(\mathbf{u}) = w_{ij} |u_i - u_j|^{p-2}$ and $b_{ij}(\mathbf{u}) = w_{i,j+n} |u_i - g_j|^{p-2}$, and

$$(2.4) \quad d_i(\mathbf{u}) = \sum_{j=1}^n a_{ij}(\mathbf{u}) + \sum_{j=1}^m b_{ij}(\mathbf{u}).$$

Then, we write $A(\mathbf{u}) = (a_{ij}(\mathbf{u}))_{ij} \in \mathbb{R}^{n \times n}$, $B(\mathbf{u}) = (b_{ij}(\mathbf{u}))_{ij} \in \mathbb{R}^{n \times m}$ and $D(\mathbf{u}) = \text{diag}(d_i(\mathbf{u})) \in \mathbb{R}^{n \times n}$. Then we can rewrite (2.3) as

$$(2.5) \quad \left(D(\mathbf{u}^k) - A(\mathbf{u}^k) \right) \mathbf{u}^{k+1} = B(\mathbf{u}^k) \mathbf{g} + \mathbf{f}.$$

Defining the matrix $L(\mathbf{u}) := D(\mathbf{u}) - A(\mathbf{u})$, the update formula becomes

$$(2.6) \quad \mathbf{u}^{k+1} = L(\mathbf{u}^k)^{-1} \left(B(\mathbf{u}^k) \mathbf{g} + \mathbf{f} \right).$$

The cost of each iteration is dominated by the cost of inverting the symmetric positive semi-definite matrix $L(\mathbf{u}^k)$.

2.2. Newton's Method. Since J_p is smooth and convex for $p \geq 2$, we consider Newton's method

$$(2.7) \quad \mathbf{u}^{k+1} = \mathbf{u}^k - \left[\nabla^2 J_p(\mathbf{u}^k) \right]^{-1} \nabla J_p(\mathbf{u}^k).$$

We compute

$$\nabla J_p(\mathbf{u}) = L(\mathbf{u})\mathbf{u} - B(\mathbf{u})\mathbf{g} + \mathbf{f} \quad \text{and} \quad \nabla^2 J_p(\mathbf{u}) = (p-1)L(\mathbf{u}),$$

and thus the Newton update is given by

$$(2.8) \quad \mathbf{u}^{k+1} = \frac{p-2}{p-1} \mathbf{u}^k + \frac{1}{p-1} L(\mathbf{u}^k)^{-1} \left[B(\mathbf{u}^k) \mathbf{g} - \mathbf{f} \right].$$

In view of (2.6), the Newton update is an underrelaxed IRLS step. By the Newton-Kantorovich Theorem [37], Newton's method is guaranteed to converge provided the initial guess is sufficiently close to the true solution. Since J_p is convex, but not strongly convex for $p > 2$, convergence may not be quadratic.

2.2.1. Convergence Rate for Star Graph. In order to better understand the convergence rate of Newton's method, we derive it analytically for a special case. Consider an *unweighted star graph*, where one node, x_{n+1} , is connected to every other node, while all other nodes are disconnected from one another. Namely,

$$w_{i,n+1} = w_{n+1,i} = 1 \quad \text{for} \quad i = 1, \dots, n+1,$$

while every other weight is zero. Suppose the graph contains $n+1$ nodes, with only one labeled node, $u_{n+1} = u(x_{n+1}) = 0$. In such case, the minimization of (2.1) reduces to

$$\min_u \frac{1}{p} \sum_{i=1}^n |u_i|^p.$$

The Newton update in this case is

$$u_i^{k+1} = u_i^k - \frac{|u_i^k|^{p-2} u_i^k}{(p-1)|u_i^k|^{p-2}} = u_i^k \left(1 - \frac{1}{p-1} \right).$$

We see that the method converges at a *linear* rate to the exact solution $u \equiv 0$. Newton's method fails to attain quadratic convergence because the function is not strongly convex near $u \equiv 0$. Looking forward to Section 3.3, we often observe quadratic convergence in practice, even though J_p is not strongly convex.

We also note that the constant in the linear rate, $\mu = 1 - 1/(p-1)$, degrades substantially as p increases. In particular, the number of steps n required to converge to within $\varepsilon > 0$ of the true solution grows linearly in p . To see this, note that N satisfies $(1 - 1/(p-1))^N = \varepsilon$, and so

$$N = \frac{\ln(\varepsilon)}{\ln(1 - 1/(p-1))} \approx (p-1) \ln(\varepsilon^{-1})$$

for large p . For more general problems, we expect Newton's method to scale at least linearly in p .

While Newton's method is successful for many problems, it has two main deficiencies. First, for larger values of p , the method can suffer from the accumulation of floating point roundoff errors from computing large exponents, and may be unstable. Second, Newton's method requires a linear solver at each iteration, which increases in complexity with n , d , and p . See Section 3.3 for an in depth discussion of the performance of Newton's method.

2.3. A primal dual approach. We present here a primal dual approach to solving the p -Laplace problem (1.15) that aims to overcome some of the shortcomings of Newton's method. The primal dual approach requires *neither the solution of a matrix system, nor raising small quantities to a large p* . Nevertheless, our experiments demonstrate this method's rate of convergence is too slow to be competitive with Newton's method. Our work in this section is based on primal dual splitting methods [10, 39, 55], which have become popular for optimization problems in image processing, and recently for obstacle problems [55].

We first introduce some notation. We define $x \sim y$ iff $w_{xy} > 0$, and define the edge set $E = \{(x, y) \in \mathcal{X} \times \mathcal{X} : x \sim y\}$. Then, we define the *gradient operator* $\nabla u \in L^2(E)$ by

$$\nabla u(x, y) = u(x) - u(y).$$

The *divergence operator* $\operatorname{div} : L^2(E) \rightarrow L^2(\mathcal{X})$ is defined as the negative adjoint of the gradient

$$(\nabla u, v)_{L^2(E)} = (-\operatorname{div}(v), u)_{L^2(\mathcal{X})}.$$

If v is skew-symmetric, that is $v(x, y) = -v(y, x)$, then (see Section A.1) the divergence is given by

$$(2.9) \quad \operatorname{div}(v)(x) = -2 \sum_{y \sim x} v(x, y).$$

Note that the gradient $\nabla u \in L^2(E)$ is skew-symmetric.

In terms of this new notation, the energy J_p defined in (1.14) can be written as

$$(2.10) \quad J_p(u, \nabla u) = \frac{1}{2p} \sum_{(x, y) \in E} w_{xy} |\nabla u(x, y)|^p + \sum_{x \in \mathcal{X}} f(x)u(x),$$

The *Legendre-Fenchel transform* of the functional J_p in the gradient variable ∇u is

$$(2.11) \quad J_p^*(u, v) := \max_{z \in L^2(E)} \left\{ (v, z)_{L^2(E)} - J_p(u, z) \right\}.$$

We show in Appendix A.2 that

$$J_p^*(u, v) = \frac{2^q}{2q} \sum_{(x, y) \in E} w_{xy}^{1-q} |v(x, y)|^q - \sum_{x \in \mathcal{X}} f(x)u(x),$$

where $\frac{1}{p} + \frac{1}{q} = 1$. In particular, $J_p^{**} = (J_p^*)^* = J_p$, as is guaranteed by convex duality [40]. Therefore, we have the equivalent *saddle point formulation*

$$(2.12) \quad \min_{u \in L^2(\mathcal{X})} J_p(u, \nabla u) = \min_{u \in L^2(\mathcal{X})} \max_{v \in L^2(E)} \left\{ (\nabla u, v)_{L^2(E)} - J_p^*(u, v) \right\}.$$

As is standard in primal-dual splitting algorithms [10, 39, 55], we solve the saddle point problem (2.12) by alternating proximal updates, as follows

$$(2.13) \quad v^{k+1} = \arg \min_{v \in L^2(E)} \left\{ -(\nabla \bar{u}^k, v)_{L^2(E)} + J_p^*(\bar{u}^k, v) + \frac{1}{2r_1} \|v - v^k\|_{L^2(E)}^2 \right\}$$

$$(2.14) \quad u^{k+1} = \arg \min_{u \in L^2(\mathcal{X})} \left\{ -(u, \operatorname{div}(v^{k+1}))_{L^2(\mathcal{X})} - J_p^*(u, v^{k+1}) + \frac{1}{2r_2} \|u - u^k\|_{L^2(\mathcal{X})}^2 \right\}$$

$$(2.15) \quad \bar{u}^{k+1} = 2u^{k+1} - u^k.$$

The variables u, v shall be known as primal and dual variables, respectively. We shall refer to the first two steps above as the dual update, and the primal update, respectively. The labels are set during the primal update, which is restricted to $u \in L^2(\mathcal{X})$ with $u = g$ on \mathcal{O} . The third step is known as an over relaxation step, while \bar{u} is the over relaxation variable. Apparent advantages of the primal dual formulation are (1) when $p > 2$, $1 < q \leq 2$, and so we avoid issues with large exponents, and (2) the method does not involve solving large linear systems.

Notice that both the primal (2.14) and dual (2.13) steps are pointwise optimization problems. The primal problem can be solved explicitly by

$$(2.16) \quad u^{k+1}(x) = u^k(x) + r_2(\operatorname{div} v^{k+1}(x) - f(x)),$$

for $x \in \mathcal{X} \setminus \mathcal{O}$, and $u^{k+1}(x) = g(x)$ for $x \in \mathcal{O}$. The dual problem is independent of the term $f(x)u(x)$ and may be written pointwise, for fixed $(x, y) \in E$, as

$$(2.17) \quad v^{k+1}(x, y) = \arg \min_{v \in \mathbb{R}} \left\{ -(\bar{u}^k(x) - \bar{u}^k(y))v + \frac{2^q}{2q} w_{xy}^{1-q} |v|^q + \frac{1}{2r_1} (v - v^k(x, y))^2 \right\}.$$

The minimization problem (2.17) cannot be solved explicitly, and solving it efficiently is the bottleneck of the primal dual method. We solve the dual problem with a bisection search—for details see Appendix A.4. Alternatively, we can approximately solve (2.17) with one step of gradient descent, yielding the explicit update

$$(2.18) \quad v^{k+1}(x, y) = v^k(x, y) + \delta \left(\bar{u}^k(x) - \bar{u}^k(y) - 2^{q-1} w_{xy}^{1-q} |v^k(x, y)|^{q-1} \operatorname{sign}(v^k(x, y)) \right),$$

where δ is a step size to be specified. In our experiments, we set $\delta = r_1$.

We also note that if v^0 is skew-symmetric, then v^k is skew-symmetric for all $k \geq 1$ (see Appendix A.3), and so formula (2.9) can be used in the primal update (2.16). A convergence rate of order $O(1/N)$, where N is the number of iterations, has been proved in [39], for fixed r_1, r_2 satisfying

$$(2.19) \quad r_1 r_2 \|\nabla\|^2 \leq 1.$$

In our case we have

$$\|\nabla\|^2 = \sup_{\|u\|=1} \sum_{(x,y) \in E} (u(x) - u(y))^2 \leq 2 \sup_{\|u\|=1} \sum_{(x,y) \in E} u(x)^2 + u(y)^2 \leq 4K',$$

where K' is the maximum number of neighbors a given $x \in \mathcal{X}$ has. We define a parameter γ , and set these step sizes r_1, r_2 according to

$$(2.20) \quad r_1 = \gamma^{-1} \frac{\rho}{\sqrt{4K'}} \quad \text{and} \quad r_2 = \gamma \frac{\rho}{\sqrt{4K'}},$$

where $\rho \leq 1$. Experiments examine the effect of different choices of ρ, γ on the convergence rate.

3. NUMERICAL EXPERIMENTS FOR THE VARIATIONAL PROBLEM

We now present numerical results for computing solutions of the variational p -Laplace equation. Section 3.1 details the experiments we shall report on in this section, while Sections 3.2, 3.3 and 3.4 provide results for each of the algorithms we have proposed. Our final assessment among all schemes we considered for solving the variational problem is discussed in Section 3.5.

3.1. Description of Numerical Experiments. We describe here the experiments that will be used to test the accuracy and performance of our methods for the variational problem. These experiments will also be used later in the paper for the game theoretic problem in Section 5.

Problem A. For the purpose of testing the accuracy of a method in two dimensions, we first consider solving (1.15) for the exact solution $u_e : \mathbb{R}^2 \rightarrow \mathbb{R}$

$$(A) \quad u_e(x) = 3(1 - x_1)^2 e^{-x_1^2 - (x_2+1)^2} - 10 \left(\frac{x_1}{5} - x_1^3 - x_2^5 \right) e^{-x_1^2 - x_2^2} - \frac{1}{3} e^{-(x_1+1)^2 - x_2^2},$$

where $x = (x_1, x_2) \in \mathbb{R}^2$. This function is plotted in Fig. 2 for 10,000 vertices randomly sampled in $[-3, 3]$. The corresponding function $f : \mathcal{X} \setminus \mathcal{O} \rightarrow \mathbb{R}$ is computed from (1.15) via the forward operator $f := -\Delta_p^G u_e$. In all our experiments, we only label one vertex ($m = 1$).

Problem B. In order to test accuracy for higher dimensional problems, we consider solving (1.15) in 10 dimensions. We define the exact solution $u_e : \mathbb{R}^{10} \rightarrow \mathbb{R}$ by

$$(B) \quad u_e(x) = x_1^2 - x_2^3 + 10x_3 - \sin(10x_4) + e^{x_5} - \cos(x_6 x_7) - x_8^{x_9} + |x_9 - x_{10}|.$$

As for Problem A, we compute f via the forward operator $f := -\Delta_p^G u_e$, and use $m = 1$.

Problem C. We consider here the problem from Figure 1. That is, in two dimensions, we label two extreme points ($m = 2$)

$$(C) \quad g(1/2, 1) = 1, \quad \text{and} \quad g(1/2, 0) = 0,$$

and sample n unlabeled points from a uniform distribution on $[0, 1] \times [0, 1]$.

Problem D. We now consider a higher dimensional version of Problem C, where we sample \mathcal{X} from a uniform distribution on $[0, 1]^d$. We set $m = 10$ and pick 10 points y^1, \dots, y^{10} randomly in $[0, 1]^d$ and assign random labels

$$(D) \quad g(y^i) = \ell^i, \quad i = 1, \dots, 10,$$

where ℓ^i are randomly sampled from a uniform distribution on $[0, 1]$. The main purpose of testing a higher dimensional problem is to examine how the computational cost increases. The experiments we report on use $d = 5$ and $d = 10$, as the computational cost did not increase for $d > 10$.

Problems A and B are primarily used to show that a given algorithm converges to an exact solution, but problems C, D are the ones we are truly interested in. They correspond to solving (1.15) for $f(x) = 0$, which means solving the p -Laplacian model; the central problem of this paper.

Relevant numerical issues for these problems are discussed below. Section 3.1.1 provides details about the weights, Section 3.1.2 describes the linear solvers, and Section 3.1.3 discusses the error metrics we report on.

3.1.1. Implementation Details. We have performed all our tests using MATLAB 2018, and the timing results have been produced on a laptop with 16GB of RAM memory. Unless stated otherwise, we have sampled our data points uniformly on a box $[0, 1]^d$, where d is the dimension of the problem.

We construct the graph by connecting every $x \in \mathcal{X}$ to $\eta(x) =$ set of K nearest neighbors. Then,

$$(3.1) \quad w_{xy} = \begin{cases} \exp\left(-\frac{\|x-y\|^2}{\sigma^2}\right), & \text{if } x \in \eta(y) \text{ or } y \in \eta(x) \\ 0, & \text{otherwise.} \end{cases}$$

The constant σ plays the role of being a *typical length scale* for the problem. In our experiments, we compute it as follows

$$(3.2) \quad \sigma = \frac{1}{2} \max \left\{ \|x - y\| \mid \text{s.t. } w_{xy} \neq 0 \right\}.$$

For the sake of consistency, we have used $K = 10$ throughout all experiments. Any choice of K for which the graph is connected should not affect the results in any significant way. However, as K increases the computational cost increases. The only requirement is that K needs to be large enough to ensure the graph is connected. It should be noted that, even though we prescribe $K = 10$,

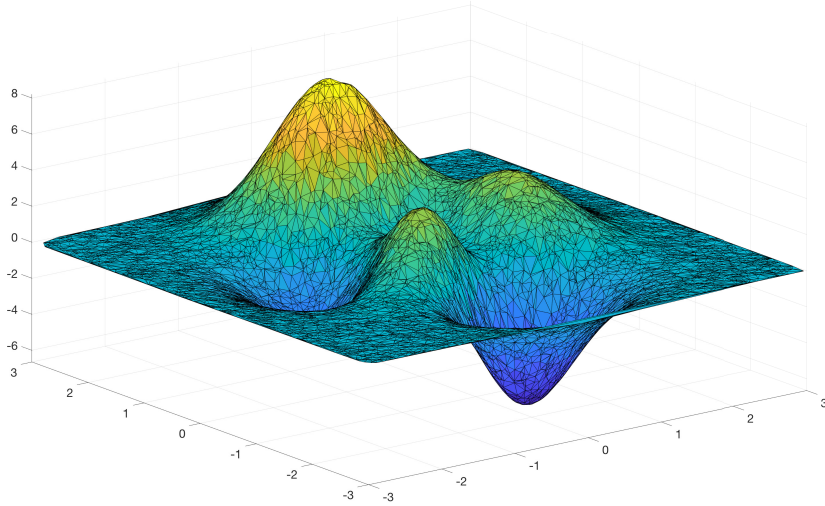


FIGURE 2. This two dimensional function, given by equation (A), is obtained by translating and scaling Gaussian distributions. This is a standard function within MATLAB software, known as *peaks*. We shall use this function as an exact solution to (1.15), to test the accuracy of each algorithm in $2d$.

after we apply (3.1), most vertices will have a higher number of neighbors (so that symmetry can be enforced). For notation, let K' be a bound on the number of neighbors of any vertex in the graph.

3.1.2. *Linear Solver.* We explored direct and indirect solvers for inverting $L(\mathbf{u})$ in (2.6) and (2.8).

For a direct solver, we used MATLAB's built-in backslash operator. Given that $L(\mathbf{u}^k)$ is symmetric positive semidefinite matrix, a Cholesky factorization with pivoting (see, for example, [25]) is the optimal approach, and is automatically selected by MATLAB in an overwhelming majority of cases. As p gets larger (e.g. $p > 30$), roundoff errors may sometimes eliminate the positive semidefinite property, hence requiring an \mathcal{LDL}^T factorization instead. In MATLAB, such routine is known as MA57, and it is approximately 3 times slower than Cholesky, see [14] for details.

For an indirect solver, we used MATLAB's preconditioned conjugate gradients method (PCG), with an incomplete Cholesky factorization (IC) as a preconditioner (see Section 3.3.4).

3.1.3. *Error Reporting.* In the case of problems A and B, we have an exact solution u_e available. Numerical experiments on problems A or B report an absolute error

$$(3.3) \quad \epsilon := \max_{x \in \mathcal{X}} |u(x) - u_e(x)|.$$

Meanwhile, problems C and D do not possess an exact solution, hence for these problems we report

$$(3.4) \quad \epsilon = \frac{1}{n\sigma^{d+p-1}} \max_{x \in \mathcal{X}} |\Delta_p^G u(x)|,$$

which amounts to scaling the largest residual in equation (1.13), by the number of points, and the typical length scale σ , given by (3.2). This scaling ensures a fair comparison across different n, p, d .

3.2. **Numerical Results for IRLS.** First we test the accuracy of IRLS in solving problem A for $p = 2.5$. The input to our simulation is: a vertex set $\mathcal{X} \subset \mathbb{R}^2$ (randomly sampled from a uniform distribution on $[-3, 3] \times [-3, 3]$), the function f computed at each $x \in \mathcal{X}$ according to (1.15).

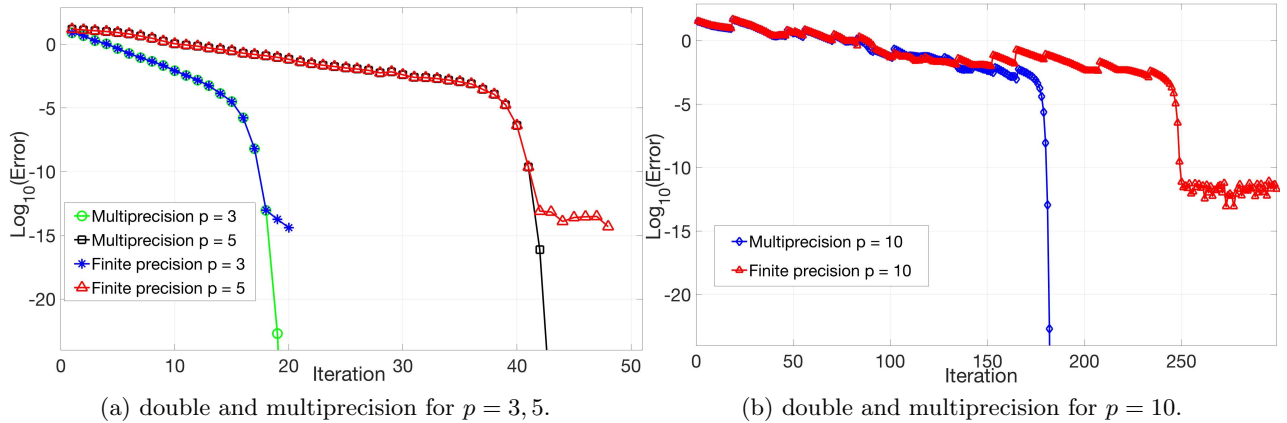


FIGURE 3. Newton's convergence for problem A with $n = 10^3, m = 1$.

- (a) Both double and multiprecision achieve quadratic convergence near the solution.
 (b) Multiprecision converges faster, since roundoff errors become more serious.

That is, for the m labeled points $g(x) = u_c(x)$ and for the n unlabeled points one needs to solve $\Delta_p^G u(x) = f(x)$. We used $n = 10^3, m = 1, K = 10$, with tolerance $\epsilon < 10^{-12}$.

IRLS is able to reach the desired accuracy within 45 iterations, but repeating this experiment for problems with $p > 3$ invariably leads to failure. For example, for $p = 3.5$, this algorithm diverges in under 10 iterations. Similar deficiencies have been previously documented in IRLS literature.

Our experiments have led us to believe that IRLS may produce successful results for $p < 3$, but will fail for $p > 3$ and therefore, we will no longer consider this algorithm in subsequent sections.

3.3. Numerical Results for Newton's method. Our experiments are organized as follows: Section 3.3.1 tests the accuracy of the algorithm, by solving problems A, B, while Section 3.3.2 discusses how the iteration count increases with p . A systematic approach to producing good initial guesses is presented in Section 3.3.3, and demonstrated with problem D. The computational cost of the method is discussed in Section 3.3.4. We summarize our conclusions in 3.3.5.

3.3.1. Testing Newton's Accuracy. We repeat the previous experiment using Newton's method. We solve (1.15), to an accuracy of $\epsilon < 10^{-12}$, in 20 iterations for $p = 3$, and 48 iterations for $p = 5$. Newton's method takes much longer to achieve a comparable level of accuracy for larger p . For example, the same experiment took 250 iterations to reach an accuracy of 10^{-12} when $p = 10$.

In order to better understand the impact of roundoff errors, we implemented Newton's method in arbitrary precision, using the Advanpix library. We repeated the experiment above for $p = 3, 5, 10$, using 32 digits of accuracy, and compare results in Figure 3. Newton's method, with finite precision, exhibits quadratic convergence for $p = 3$ and $p = 5$, and to a lesser extent for $p = 10$, where roundoff errors play a bigger role, and the multiprecision implementation outperforms (see Figure 3b).

Although arbitrary accuracy appears to help, even 160 digits of accuracy are not enough to achieve convergence for problem A for $p = 20$, unless a good initial guess \mathbf{u}^0 is available. The instability we see in Figure 3b, where the error occasionally increases by a large margin, becomes more serious with larger p . We address the issue of choosing a good \mathbf{u}^0 in Section 3.3.3.

We obtained similar results when solving problem B, where we sampled data points from a uniform distribution on $[0, 1]^{10}$, and set $n = 10^4, m = 1, \epsilon < 10^{-12}$. We need 22 iterations for $p = 3$, and 83 for $p = 5$. We fail to reach $\epsilon < 10^{-12}$ when $p = 10$, which further exemplifies the need for good initial guesses. The results (and iteration counts) in Section 3.3.3 shall be much better.

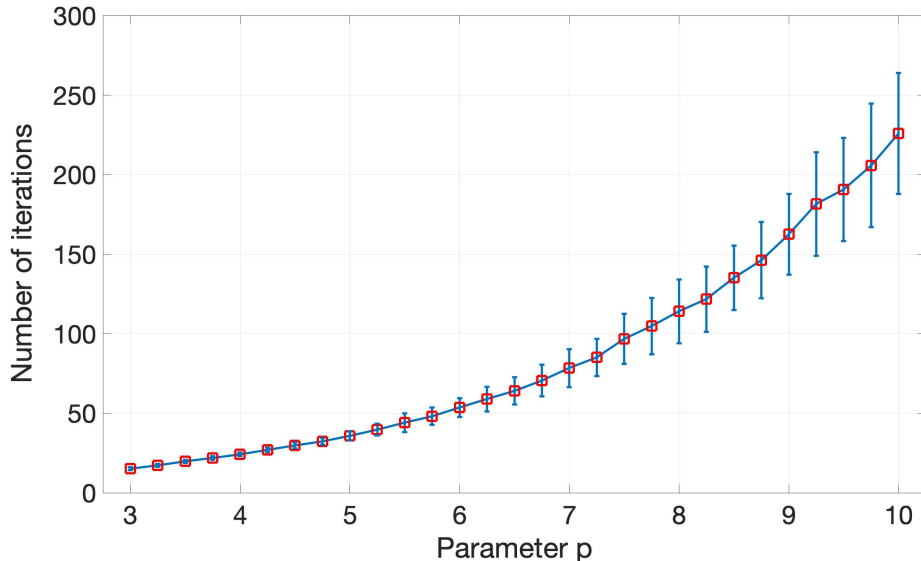


FIGURE 4. Demonstration of the number of iterations for solving problem A as a function of p . Iterations are performed until the accuracy is below 10^{-6} and their number is averaged over 100 experiments. This average increases with p according to a power law with exponent 2.35. Error bars indicate one standard deviation.

3.3.2. *Iteration count vs. p .* In Section 2.2.1 we considered a very simple graph, and showed that the number of iterations required to reach a given accuracy increased linearly with p in that setting. Given the simplicity of the case we considered, such scaling should be a lower bound. We explored this dependence in a more general setting by solving problem A, for $p \in [3, 10]$ in increments of $1/4$, with $n = 10^3$ and $m = 10$. We set a tolerance of $\epsilon < 10^{-6}$, and report the number of iterations needed.

We repeated this experiment 100 times, with different randomly sampled vertex sets \mathcal{X} , to account for slightly easier/harder configurations. In Figure 4, we report the average number of iterations, alongside error bars representing one standard deviation. The iteration count is slightly worse than quadratic in p .

3.3.3. *Homotopy on p .* Previous sections discuss the performance of Newton’s method without specifying how \mathbf{u}^0 is chosen. Starting from $\mathbf{u}^0 = 0$ is impossible, because every entry in $L(\mathbf{u}^0)$ would be zero, hence previous experiments randomly sampled \mathbf{u}_0 from a Gaussian distribution.

One can significantly improve the choice of \mathbf{u}_0 by noting two features in Newton’s method.

- (1) The problem (1.13), with $p = 2$ can be solved exactly with only one matrix inversion.
- (2) Most of the computational cost comes from approaching the solution. Once we reach the quadratic convergence region, Newton only requires a handful of steps to converge.

As a result, we can solve (1.13), with $p = 3$ more efficiently by first setting \mathbf{u}_0 to be the solution of the $p = 2$ problem. Furthermore, if we wish to solve (1.13), with a much larger value of p , we can do so in steps, compute the solution for $p = 2$, use it to compute $p = 3$, then perhaps $p = 5, 10$, etc. This approach is known in the literature as homotopy, and has been applied to a variety of problems in order to improve performance on related problems. For example, see [20, 45].

Homotopy is very effective at improving the performance and reliability of Newton’s method for higher p . We illustrate the value of homotopy by solving Problem D, a 10-dimensional problem, for $p = 50$, by first solving it for $p = 2$ (which only requires 1 iteration), and using that result as

N	p										
	3	4	6	8	10	15	20	25	30	40	50
1	2e-01	3e-02	1e-02	8e-04	2e-04	8e-05	4e-06	3e-07	3e-08	1e-09	2e-11
2	5e-02	3e-03	4e-04	1e-05	7e-07	1e-06	2e-08	6e-10	3e-11	5e-12	3e-14
3	7e-03	2e-04	4e-05	7e-08	2e-10	3e-10	3e-13	4e-15	1e-16	9e-17	-
4	8e-04	1e-05	4e-06	2e-09	1e-13	2e-14	-	-	-	-	-
5	5e-05	4e-07	8e-07	5e-12	-	-	-	-	-	-	-
6	4e-07	1e-09	7e-08	2e-16	-	-	-	-	-	-	-
7	2e-11	2e-14	6e-10	-	-	-	-	-	-	-	-
8	8e-15	-	1e-12	-	-	-	-	-	-	-	-
9	-	-	2e-16	-	-	-	-	-	-	-	-

TABLE 1. Demonstration of Newton’s method with homotopy for solving problem D. Homotopy allows us to solve this problem with $p = 50$ and $\epsilon < 10^{-12}$ in a total of 56 iterations. We can take increasing steps in p while remaining in the quadratic convergence regime, suggesting we could go much farther than $p = 50$.

\mathbf{u}^0 for the $p = 3$ problem. The process is repeated with increasing step sizes in p , until $p = 50$ is reached. We used $m = 10$ and $n = 10^4$ points, and require $\epsilon < 10^{-12}$ according to (3.4). Table 1 reports ϵ at each iteration.

Given that no exact solution is available for the problem we are solving, and the accuracy level we report (meaning ϵ) is limited by our ability to compute that quantity accurately in the first place; we have used our multiprecision implementation to confirm the quality of our results. We performed a homotopy experiment, side by side, with 100 digits of accuracy, to compute an *exact* solution to these problems for each p value. Later, we computed the difference between the finite precision answer, and the multiprecision answer. We were able to verify that, even for $p = 50$, our solutions have reached the accuracy we appear to have in Table 1. In later experiments we automate the homotopy process through a simple iteration in p , by defining a step size, as well as a rejection criteria. We suggest setting $p^0 = 2$, and approach the target p with the iteration

$$(3.5) \quad p^{j+1} = \max\{1.5 \cdot p^j, p\}.$$

At each iteration in j , we may reject the p^j value if Newton’s method requires more than N_0 iterations to achieve machine precision for that problem, in which case we can take a smaller step in p (e.g. $p^{j+1} = 1.25 \cdot p^j$). We recommend choosing $N_0 = 10$.

3.3.4. Computational Cost. We explore the computational cost of using Newton’s method with homotopy, according to (3.5), for solving (1.13), for different problem sizes. We solved the problem for $p = 11$ until $\epsilon < 10^{-7}$, according to (3.4). In all cases, we set $m = 10$ and sampled points from a uniform distribution on $[0, 1]^d$. We varied n and d , and report the time required in Figure 5a.

The results shown in Figure 5a shows that the cost of Newton’s method with a direct solver increases by a factor of 100 going from $d = 2$ up to $d = 10$. This happens even though the only place in which d appears in our problem is in the definition of the weights w_{xy} . We attribute this dramatic increase in computational cost to the increasing bandwidth of the underlying matrix system. We improve performance in higher dimensions by solving the linear system using conjugate gradient (CG). Performance benefits greatly from using \mathbf{u}^k as a starting guess when using CG to solve for \mathbf{u}^{k+1} . Given that the linear system is symmetric, we chose Incomplete Cholesky as a preconditioner, and specified a drop tolerance of 10^{-1} , which allows to preserve a great deal of sparsity in the Cholesky factorization. At each iteration, we set the tolerance of CG to be 1% of the current residual. As we can see in Figure 5a, the iterative solver is slower than the direct one for $d = 2$, but dramatically faster in higher dimensions.

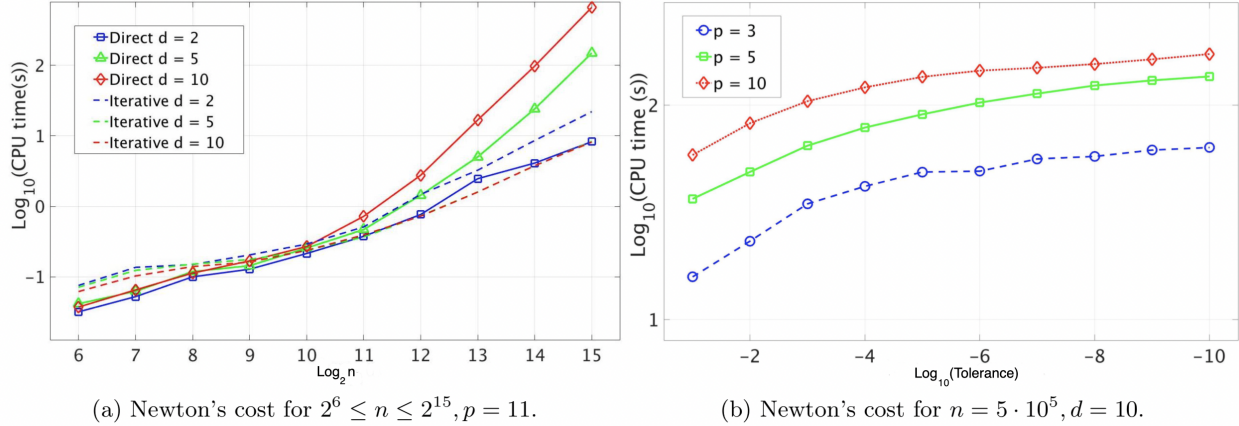
(a) Newton's cost for $2^6 \leq n \leq 2^{15}$, $p = 11$.(b) Newton's cost for $n = 5 \cdot 10^5$, $d = 10$.

FIGURE 5. Newton's cost in solving problem D. (a) We measure Newton's cost until $\epsilon < 10^{-7}$, and compare preconditioned CG with MATLAB's backslash solver. (b) Newton's cost to reach a given tolerance, using preconditioned CG, for $n = 5 \cdot 10^5$.

We also confirm our ability to solve large scale problems by solving problem D with $m = 10$, $K = 10$, $n = 5 \cdot 10^5$, in 10 dimensions, using Newton's, for $p = 3, 5$ and 10, starting from the solution to the $p = 2$ problem. We plot the result in Figure 5b.

3.3.5. Summary of Results for Newton's method. The results discussed in this section make a strong case for Newton's ability to solve (1.13), at least for problems with moderate p values. Perhaps the most important issue our experiments have raised is the importance of having a good initial guess. Homotopy is the natural solution to this problem, and in all the experiments we have performed, homotopy has proven to be fundamental if our goal is reaching high p values.

The biggest deficiency in Newton's method is its difficulty in dealing with larger values of p . In terms of computational cost, we have seen that, without homotopy, the iteration counts increase at least linearly with the p value, while using homotopy creates a need to solve (1.13) repeatedly until reaching the desired p value. Homotopy is strongly recommended to deal with larger p values, but the computational cost is still an issue for large p . Beyond this computational limitation, as p gets very large, roundoff errors become a serious concern.

On the positive side, the cost of each iteration with an iterative solver, increases slightly faster than $O(n)$, while the dimension d does not have a strong effect on the CPU time.

3.4. Numerical Results for the Primal Dual Method. We test the method's accuracy in 3.4.1, and then discuss its convergence rate and parameter tuning in 3.4.2. We report computational performance in Section 3.4.3, and summarize our findings in 3.4.4.

3.4.1. Testing the Accuracy of the Primal Dual method. We solved problem A for $p = 3$, with $n = 10^3$, $m = 1$. We chose $\gamma = 10$, and solved the dual step to high accuracy by using 50 bisection steps. We reached an accuracy of $\epsilon < 10^{-12}$ after 14,500 iterations. The problem became harder with larger p . For example, for $p = 5$ and still choosing $\gamma = 10$, the method converged very slowly and took over 50,000 iterations to achieve $\epsilon < 10^{-1}$. Similar results were obtained when solving Problem B; convergence is steady, but very slow.

From these experiments, we concluded that this algorithm can reliably converge to an accurate solution, but given the extremely slow convergence rate, it is essential to find ways to increase convergence rate, or reduce the cost of each iteration.

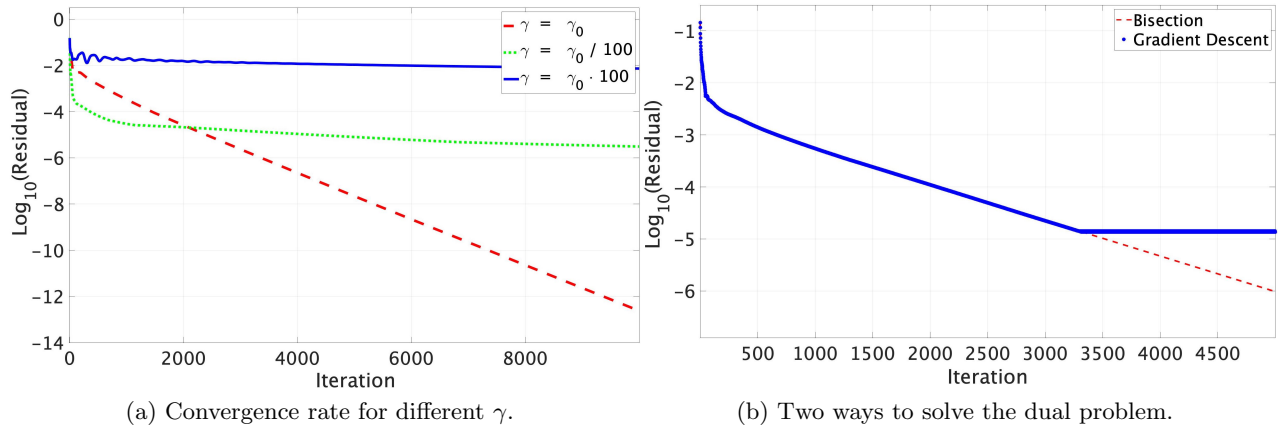


FIGURE 6. Demonstration of numerical strategies for speeding up the primal-dual solution. (a) Solve problem C, for $p = 3$, $n = 5000$, $m = 10$, and observe a linear convergence rate when $\gamma = \gamma_0 := n^{1/d} \cdot 10^{2p-5}$. (b) Solve problem C, for $p = 3$, $n = 10^4$, $\gamma = \gamma_0$, with two different solvers for the dual problem. For $\epsilon > 10^{-5}$, using a single gradient descent step (which is much faster) works just as well as bisection (which is exact, but slow).

3.4.2. *Tuning the parameter γ .* When this primal dual approach was first proposed in [39], a worst-case convergence rate of $O(1/N)$ was proven, where N is the number of iterations. A requirement for this convergence rate was that r_1, r_2 satisfy the condition (2.19), which in our case reduces to $\rho \leq 1$ in (2.20). The bound does not tell us anything about how γ should be chosen in (2.20). Our experiments have shown it is possible to obtain a faster order of convergence if γ is accurately tuned. Unfortunately, an optimal choice for γ, ρ , would likely be problem-dependent, explaining why little has been said about tuning these parameters in general. For example, in [55], the authors provide three examples, each with their own r_1, r_2 , but no details are provided on how these parameters were chosen. Using our notation, these examples used $\gamma = 50, 35$ and 44 respectively.

Choosing appropriate step sizes r_1, r_2 by trial and error could be an arduous job, and we performed a large variety of tests in an attempt to provide some guideline for choosing the appropriate γ . Intuitively, γ is the speed in which information propagates throughout the graph. For this reason, it is natural to assume that γ should be inversely proportional to σ , the typical length scale of the problem; see equation (3.2). For a fixed K , and assuming data points are uniformly sampled in d dimensions, the proper scaling is $\gamma \sim n^{1/d}$. A series of two dimensional experiments, using $p = 3$ together with a high accuracy dual step (50 steps of the bisection method) with $n = 10^2, 10^3, 10^4, 10^5$, as well as parameters $\gamma = 10^{-1}, 1, 10, 10^2, 10^3, 10^4, 10^5$ helped us to conclude that this proportionality is suitable. Our experiments suggested that $\gamma = n^{1/d} \cdot 10^{2p-5}$ is a viable ad-hoc formula, for this setting. One should expect that this formula only works on the specific setting we have tested, but at least we have observed that tuning γ effectively is possible.

We illustrate the importance of tuning γ carefully, by solving problem C for $p = 3$, with $n = 5,000$ and $m = 10$. We define $\gamma_0 := n^{1/d} \cdot 10^{2p-5}$, and used three choices for γ , namely $\gamma = \gamma_0, \gamma_0/100, 100\gamma_0$. We plot the residual at each iteration in Figure 6a. As we can see from the plot, using $\gamma = \gamma_0$ provided results in a linear convergence rate, while $\gamma = \gamma_0/100$ results in the $O(1/N)$ rate that was predicted by [39]. Choosing $\gamma = 100\gamma_0$ makes the residual oscillate for about 1000 iterations before falling into a much more disadvantaged $O(1/N)$ convergence regime (worse than $\gamma = \gamma_0/100$). It may be possible to interpret $1/\gamma$ as a damping parameter, with $\gamma = 100\gamma_0$ being underdamped (causing the oscillations), while $\gamma = \gamma_0/100$ is overdamped, causing the slow convergence.

Figure 6a helps to visualize how slow a $O(1/N)$ convergence rate really is. The green curve gains a couple orders of magnitude within the first hundred 500 iterations, and makes almost no progress for the subsequent 9,500 iterations. The blue curve fails to gain much at the start, and is essentially never going to reach the accuracy achieved by the green curve within the first 500 steps.

3.4.3. Computational Cost. Given that the primal update is explicit, the cost of each iteration is dominated by the cost of solving (A.2), which appears later in the Appendix. Even after we exclude the pairs (x, y) that do not need solving, this problem still accounts for about 90% of the total cost of an iteration. Two approaches to reduce the cost of individual iterations are

- (1) Solving (A.2) to a lower precision, for example, by using only 20 bisection steps.
- (2) Replacing the bisection method by a single gradient descent step, according to (2.18).

Both approaches are viable, and we have found that, at least initially, using gradient descent steps does not negatively impact convergence. For example, we solved Problem C, with $n = 10^4$ with $m = 10$ and $p = 3$. We picked $\gamma = n^{1/d} \cdot 10^{2p-5}$, and compared the performance of our algorithm using both a bisection method with 50 steps, and a simple gradient descent step. We plot the maximum residual of (1.13) in Fig. 6b. Using a single gradient step produces almost the same quality of result as an exact dual step solve, but is about 10 times faster. Our numerical experiments consistently result in a similar picture; a single gradient step will produce nearly the same convergence rate, but eventually stagnate, due to the limited accuracy to which the dual step is being solved. Further improvements could be achieved by replacing the gradient step with a bisection method once a given accuracy has been reached.

In Section 3.3.4 we noted how the cost of inverting the Hessian matrix for $d = 10$, using a direct solver, increases the computational cost so that it can be as much as 100 times the cost of inverting the system for a two dimensional problem. We overcame this issue using an indirect solver.

The intrinsic dimensionality of the problem only has a weak impact in the performance of the Primal Dual method, as it increases the number of (x, y) pairs for which the dual step needs to be solved. Our timing tests have established that the computational cost only increases by about a factor of 3, when going from $d = 2$ up to $d = 10$, irrespective of n . This scaling is much better than Newton’s method with a direct solver, but worse than Newton’s method with an indirect solver.

3.4.4. Summary of Results for the Primal Dual method. Our numerical experiments suggest that our algorithm can produce accurate solutions, but its convergence rate is too slow to be used in practice, unless a substantial speedup can be found. Solving the dual step inexactly is a simple way to gain speed, but it seems that the key to a successful use of the primal dual method is a carefully tuned γ parameter. The formula we provided, $\gamma = n^{1/d} \cdot 10^{2p-5}$ worked well in the synthetic experiments we considered, but different problems would likely require a different choice.

3.5. Variational Solvers Summary. We have examined three algorithms, namely IRLS, Newton and Primal Dual. We discarded IRLS due to its inability to reliably handle $p > 3$.

The suitability of Newton’s method hinges upon two key factors; its computational scalability for high n, p, d , and the difficulty in producing a viable initial guess. The use of an indirect solver is essential in dealing with problems with large n, d . Meanwhile, using homotopy helps to produce reliable initial guesses, and due to Newton’s quadratic convergence rate near a solution, this approach produces accurate solutions for large p in a moderate amount of time. The need to compute $|u(x) - u(y)|^p$ for very large p , and the associated roundoff errors, are a significant concern. The matrix $L(\mathbf{u}^k)$ may be inaccurately constructed, and the residual error at each iteration may be inaccurately computed, making it difficult to find a reliable stopping point.

At first sight, the primal dual approach appears to solve some of these concerns. There is no need to compute large powers of p , and no need to invert a linear system. In addition, the most expensive step can be easily parallelized. A major disadvantage of this approach is its slow convergence rate of $O(1/N)$. An optimal choice of γ may produce a linear convergence rate, but an appropriately tuned

parameter may be hard to find in some cases. Given that [39] has proven an $O(1/N)$ convergence rate even for $\gamma = 1$, we are confident this algorithm can produce a reasonable solution regardless of the choice of γ , but convergence is likely to be too slow for any large scale problem.

Overall, we have two viable approaches for solving the variational formulation, but Newton's method with homotopy is the clear winner, due to its fast convergence rate, and ease of use, without the need for parameter tuning.

4. ALGORITHMS FOR GAME THEORETIC PROBLEM

We now consider algorithms for solving the game theoretic problem (1.16). We shall discuss a gradient descent-type method in Section 4.1. In Section 4.2 we describe a Newton-like algorithm, while Section 4.3 discusses a semi-implicit method. Numerical results begin in Section 5.

4.1. Gradient Descent Approach. The simplest approach to solving (1.16) is the gradient descent-type scheme

$$(4.1) \quad u^{k+1}(x) = u^k(x) + \alpha(\mathcal{L}_p^G u^k(x) + f(x)).$$

The scheme is *monotone* if all coefficients in front of u^k on the right hand side are positive. For a specific x , let $y = y_1$ be the minimizer of $w_{xy}(u^{k+1}(x) - u^k(y))$ and $y = y_2$ be the maximizer. Then, we can write (4.1) as

$$u^{k+1} = u^k(x) \left(1 - \frac{\alpha}{p}\right) + \frac{\alpha}{d_x p} \sum_{y \in \mathcal{X}} w_{xy} u^k(y) - \alpha \left(1 - \frac{2}{p}\right) \left[w_{xy_1} (u^k(x) - u^k(y_1)) + w_{xy_2} (u^k(x) - u^k(y_2)) \right].$$

Every coefficient of $u^k(y)$ for $y \neq x$ is positive if $\alpha > 0$. Combining terms in front of $u^k(x)$, we conclude that the scheme is monotone provided

$$1 - \frac{\alpha}{p} - \alpha \left(1 - \frac{2}{p}\right) (w_{xy_1} + w_{xy_2}) > 0.$$

Since $w_{xy_1} + w_{xy_2} < 2$ we obtain the time-step bound $\alpha < p/(2p - 3)$, which ensures the scheme is monotone, and hence stable. This bound is similar to a CFL condition in numerical PDEs. Convergence of this gradient descent algorithm with a linear rate was proved in [21] with a contraction argument.

4.2. A Newton-like Algorithm. We now consider a Newton-like method for solving (1.16). Newton's method is based on iteratively solving the linearization. In order to linearize (1.16), we define y_+^k and y_-^k by

$$(4.2) \quad \begin{aligned} y_+^k(x) &\in \operatorname{argmax} w_{xy} (u^k(x) - u^k(y)) \\ y_-^k(x) &\in \operatorname{argmin} w_{xy} (u^k(x) - u^k(y)), \end{aligned}$$

and then introduce the β_{xy}^k coefficients defined by

$$(4.3) \quad \beta_{xy}^k = w_{xy} \left(1 + d_x(p - 2) [\delta_{y=y_+^k} + \delta_{y=y_-^k}]\right).$$

We also define

$$(4.4) \quad \mathcal{L}_{p,k}^G u(x) := \frac{1}{d_x p} \sum_y \beta_{xy}^k (u(y) - u(x)).$$

The Newton-like iteration computes u^{k+1} as the solution of

$$(4.5) \quad \begin{cases} -\mathcal{L}_{p,k}^G u^{k+1}(x) = f(x) & \text{if } x \in \mathcal{X} \setminus \mathcal{O} \\ u(x) = g(x) & \text{if } x \in \mathcal{O}, \end{cases}$$

We note that if $y_{\pm}^{k+1} = y_{\pm}^k(x)$ for all x , then $f = -\mathcal{L}_{p,k}^G u^{k+1} = -\mathcal{L}_p^G u^{k+1}$. Hence, we obtain convergence to the exact solution as soon as the locations of the min and max in (4.2) are correct, which happens in a finite number of iterations.

4.3. Semi Implicit Approach. Here, we extend the semi-implicit method of Oberman [36] to the graph setting. Given $\theta(x) \geq 1$, we add $-\theta(x)\Delta_2^G u(x)/(2d_x)$ to both sides of (1.16), to obtain

$$-\frac{\theta(x)}{2d_x}\Delta_2^G u(x) = -\left(\frac{\theta(x)}{2d_x} - \frac{1}{d_x p}\right)\Delta_2^G u(x) + \left(1 - \frac{2}{p}\right)\Delta_{\infty}^G u(x) + f(x).$$

Solving for $\Delta_2^G u(x)$ on the left hand side reduces this equation to

$$-\Delta_2^G u(x) = -\left(\frac{\theta(x)p - 2}{\theta(x)p}\right)\Delta_2^G u(x) + \frac{2d_x}{\theta(x)p}(p - 2)\Delta_{\infty}^G u(x) + \frac{2d_x}{\theta(x)}f(x),$$

which suggests the iterative scheme

$$(4.6) \quad -\Delta_2^G u^{k+1}(x) = \beta(x)\left(2\gamma(x)\Delta_{\infty}^G u^k(x) - \Delta_2^G u^k(x)\right) + \frac{2d_x}{\theta(x)}f(x),$$

where we have defined

$$\beta(x) = \frac{\theta(x)p - 2}{\theta(x)p} \quad \text{and} \quad \gamma(x) = d_x \frac{p - 2}{\theta(x)p - 2}.$$

One fundamental advantage of the semi-implicit iteration (4.6) is that, unlike (4.5), the iteration (4.6) requires the solution of the same symmetric positive definite system at each iteration. This means we can dramatically speed up the solver, for large scale problems, by pre-computing a Cholesky factorization and using it at each iteration, or pre-computing an Incomplete Cholesky factorization, to be used as a preconditioner for CG. Another favorable feature of this scheme is the fact that the conditioning of the system is independent of p , allowing the scheme to reliably solve problems for any p .

The choice of $\theta(x)$ affects stability and convergence of the scheme. We give a heuristic argument here suggesting the iteration (4.6) is a contraction when

$$(4.7) \quad \theta(x) \geq \frac{2}{p} + d_x \left(1 - \frac{2}{p}\right) =: \eta(x).$$

Define $y_{\pm}^k(x)$ as in (4.2) and write y_{\pm} in place of $y_{\pm}^k(x)$. Noting that (4.7) implies $-1 \leq 2\gamma(x) - 1 \leq 1$, we have

$$\begin{aligned} & |2\gamma\Delta_{\infty}^G u^k(x) - \Delta_2^G u^k(x)| \\ &= \left| (2\gamma(x) - 1) \left(w_{xy_-} (u^k(y_-) - u^k(x)) + w_{xy_+} (u^k(y_+) - u^k(x)) \right) - \sum_{y \neq y_{\pm}} w_{xy} (u^k(y) - u^k(x)) \right| \\ &\leq |2\gamma(x) - 1| \left(w_{xy_-} |u^k(y_-) - u^k(x)| + w_{xy_+} |u^k(y_+) - u^k(x)| \right) + \sum_{y \neq y_{\pm}} w_{xy} |u^k(y) - u^k(x)| \\ &\leq \sum_{y \in \mathcal{X}} w_{xy} |u^k(y) - u^k(x)|. \end{aligned}$$

Therefore, for $f \equiv 0$ it follows from the definition of the iteration (4.6) that

$$\left| \sum_{y \in \mathcal{X}} w_{xy} (u^{k+1}(y) - u^{k+1}(x)) \right| \leq \beta(x) \sum_{y \in \mathcal{X}} w_{xy} |u^k(y) - u^k(x)|,$$

where $0 < \beta(x) < 1$. While this is not a contraction, it is suggestive of what we observe in practice, namely that the semi-implicit iteration is a contraction when (4.7) is satisfied. A proof of the

contraction property seems to involve a more subtle analysis of the graph problem, which we plan to pursue in a future work.

5. NUMERICAL EXPERIMENTS FOR THE GAME THEORETIC PROBLEM

The numerical experiments in this section bear close resemblance to those in 3, and many relevant details were already provided in Section 3.1. Section 5.1 describes those features in our numerical experiments, which are specific to the game-theoretic formulation. Sections 5.2, 5.3 and 5.4 report our numerical results for each of the 4 methods we propose, while 5.5 provides a time-cost comparison of the three methods, as well as a summary of our conclusions.

5.1. Description of Numerical Experiments. The numerical experiments, and implementation details in this section closely resemble those we considered in Section 3.1. For example, we still consider problems A and B to test for accuracy in solving an exact problem, and later C, D to test computational performance in general. For problems A and B we still report

$$\epsilon := \max_{x \in \mathcal{X}} |u(x) - u_\epsilon(x)|,$$

but for problems C and D, the scaling of the residual in this formulation is different, and we report

$$(5.1) \quad \epsilon = \frac{1}{\sigma} \max_{x \in \mathcal{X}} |\mathcal{L}_p^G u(x)|.$$

Unlike the matrix $L(\mathbf{u}^k)$, in (2.6) and (2.8), the system in (4.5) is not symmetric. Using MATLAB’s direct solver results in an LU factorization, which is usually twice slower than a Cholesky factorization. For a description of the MATLAB implementation of this algorithm, see [13]. For larger problems, we consider the Generalized Minimal Residual Algorithm (GMRES) [41], preconditioned with an Incomplete LU factorization. More details are provided in Section 5.3.3.

5.2. Results for Gradient Method. We do not expect a fast convergence rate, but the cost of each iteration is low, and scales well as n, d or p become larger. Solving the two dimensional problem C for $p = 3$ and $n = 1,000$, down to an accuracy of $\epsilon < 10^{-11}$ took between 2 – 4 seconds, with $\alpha = p/(2p - 3)$; approximately 10,000 – 15,000 iterations were required. Increasing d from 2 to 10, while keeping n fixed at 1,000 decreased the iteration count, by a factor of 2 and the computational cost by a factor of 3. For a comparison with other methods, see Figure 8c.

5.3. Numerical Results for Newton-like Algorithm. This method is the analogous of Newton’s method for (1.16), and the numerical results in this section support such comparison.

5.3.1. Testing the Accuracy of our Newton-like Algorithm. We solved problem A with $n = 10^4$, $m = 1$. For an initial guess, we set \mathbf{u}^0 to be a constant, equal to the mean of all labels. We reached $\epsilon < 10^{-12}$ in 19 iterations for $p = 3$, 43 iterations for $p = 4$, and 61 iterations for $p = 5$. We report the residual at each iteration in Figure 7a. Similar to Newton’s method, most of the gain in accuracy is achieved in the final 3 iterations. Next, we solved the 10-dimensional problem B with the same n, m, ϵ , and took 7 iterations for $p = 3$, 8 iterations for $p = 4$ and 11 iterations for $p = 5$. These tests confirm the algorithm’s ability to produce accurate solutions, while also providing evidence for the increasing difficulty of the problem as p increases.

5.3.2. Homotopy Results. Similar to its variational counterpart, this Newton-like algorithm has very fast convergence near a solution, but struggles to approach it, which suggests the use of homotopy. This approach also proved to be very effective in this context. For a direct comparison with the results in Section 3.3.3, we solved problem D with $n = 10^4, m = 10$, with a tolerance of $\epsilon < 10^{-12}$, given by (5.1), and report the results in Table 2. One can see that, for this Newton-like algorithm, homotopy is bit faster to converge (compare against Table 1).

N	p										
	3	4	6	8	10	15	20	25	30	40	50
1	4e-02	1e-02	9e-03	4e-03	2e-03	3e-03	1e-03	7e-04	5e-04	6e-04	3e-04
2	4e-03	3e-03	3e-03	2e-03	1e-03	3e-03	2e-03	7e-04	3e-04	9e-04	6e-04
3	1e-03	8e-04	2e-03	6e-04	5e-04	2e-03	9e-04	1e-04	9e-05	1e-04	3e-05
4	1e-04	1e-04	5e-04	5e-04	6e-05	3e-04	5e-04	3e-16	3e-16	3e-16	3e-16
5	6e-06	1e-05	9e-05	2e-04	2e-07	6e-05	3e-16	-	-	-	-
6	2e-16	2e-16	2e-16	8e-06	4e-16	3e-16	-	-	-	-	-
7	-	-	-	3e-16	-	-	-	-	-	-	-

TABLE 2. Demonstration of Newton-like method with homotopy for solving problem D. Homotopy allows us to solve this problem with $p = 50$ and $\epsilon < 10^{-12}$ in a total of 52 iterations. Similar to Newton’s method, increasing step sizes in p are possible, suggesting we could go higher in p while and still be able to converge in few iterations.

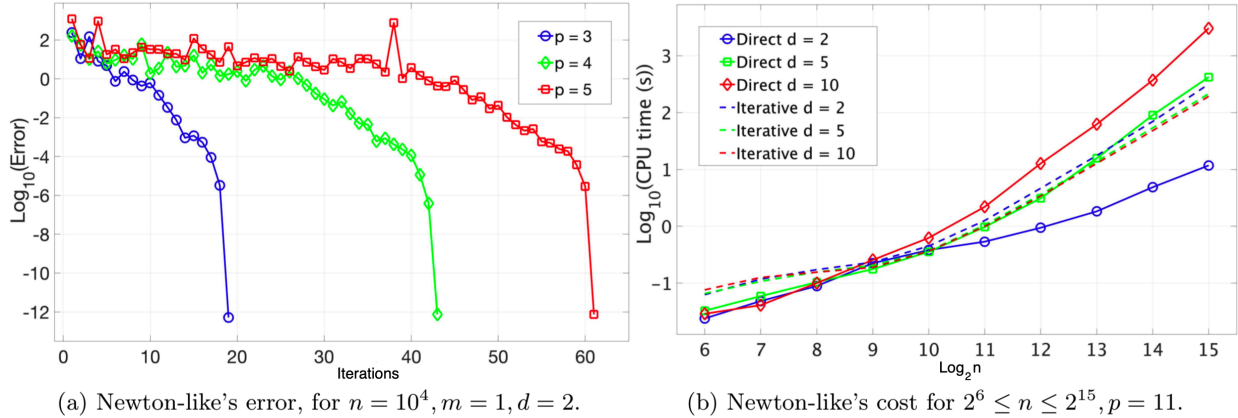


FIGURE 7. Demonstration of Newton-like’s iteration counts and computational cost. (a) We solve problem A and see the iteration count gradually increases with p . (b) We measure Newton-like’s cost in solving problem D, until $\epsilon < 10^{-7}$, and compare preconditioned GMRES with MATLAB’s backslash solver.

5.3.3. *Timing Results.* We repeated the experiment in Section 3.3.4, by solving problem D for $p = 11$, and report the CPU time in seconds, for both direct and indirect solvers in Figure 7b. A direct comparison with Figure 5b is not advisable though, as we are not solving the same problem, and the parameter p in both problems does not match exactly. As we can see from Figure 7b, varying the underlying dimension, from $d = 2$ up to $d = 10$, increases the cost of the direct solver by over $100\times$. For an indirect solver, we use a preconditioned GMRES solver, and for a preconditioner we use an Incomplete LU factorization from MATLAB’s implementation of the Crout decomposition. Since the linear system changes at each iteration, the ILU decomposition needs to be computed each time, and accounts for about $2/3$ of the total cost of each iteration, according to our numerical experiments (e.g. computing the preconditioner is more expensive than the indirect solver). Figure 7b shows that indirect solvers, while slower than a direct solver for $d = 2$, do not lose performance for higher dimensional problems, and should be used when $d > 2$.

5.3.4. *Conclusions.* Overall, this algorithm bears a strong resemblance to using Newton’s algorithm for the variational formulation, but enjoys faster convergence near a solution, and does not require the computation of large powers of p . Similar to Newton, the biggest deficiency of this algorithm

is the difficulty in finding an appropriate initial guess, and its lack of reliability far from a solution. Using homotopy resolves this problem, and results in very competitive performance.

5.4. Numerical Results for Semi-Implicit Method. Similar to other methods, we test this method’s accuracy, and then explore its convergence rate and scalability as n and d become large.

5.4.1. Testing accuracy. We solve Problem A, with $n = 10^4$ and $m = 2$. We chose $\theta(x) = 1.01\eta(x)$ (see (4.7)). This problem, with $p = 10$ took 913 iterations to reach an accuracy of 10^{-12} . We repeated this experiment for $p = 100$, and now 5,000 iterations were required to reach a tolerance of $5 \cdot 10^{-9}$. Performing a similar ten dimensional experiment on Problem B, for $p = 10$ again, took 350 iterations to reach a tolerance of 10^{-12} . All three cases exhibit a linear convergence rate.

In order to see the effectiveness of our choice of $\theta(x)$, we computed errors for four different choices, $\theta = \eta(x), 1.1\eta(x), 4\eta(x), 0.5\eta(x)$. With these four options, we solve Problem A, for $p = 10$ with $n = 10^3$, and plotted the computed error at each iteration for each one of these. We report results for the first three choices in Figure 8a, while the choice $\theta(x) = 0.5\eta(x)$ caused the algorithm to diverge very quickly. Based on the results, we can see our bound for $\theta(x)$ is effective and convergence is faster when $\theta(x)$ is close to $\eta(x)$.

These experiments, as well as others we have performed, provide strong evidence that this algorithm can provide accurate solutions in low and high dimension, for a wide range of p values.

5.4.2. Timing Results. For an accuracy of $\epsilon < 10^{-6}$, we solve D for $p = 11$, with $m = 10$, and $K = 10$, while n and d increase, and average the CPU time over 5 trials with different random vertex sets. We report our results in Figure 8b. Given that we always invert the same linear system, we compute a Cholesky factorization at the start, and use it for faster inversion at each iteration.

Similar to the timing results we performed for Newton’s method (variational formulation), and our Newton-like algorithm, the time required to invert the linear system also increases dramatically with an increasing dimension, which makes it necessary to use an indirect solver. For the semi-implicit method, we obtained excellent performance with a preconditioned CG method. Since the system does not change, we simply compute an Incomplete Cholesky factorization, with a drop tolerance of 10^{-1} , at the very beginning, and use it as our preconditioner in each iteration, saving a large amount of computational effort. Figure 8b shows the method scales very well as d increases.

5.5. Method Comparison. In order to compare the performance of different game theoretic solvers, we solved problem D with $m = 10$, $K = 10$, $n = 20,000$, and $p = 5$, in 10 dimensions, and measure the CPU time required for each method to reach an accuracy of $\epsilon < 10^{-1}, 10^{-2}, \dots, 10^{-10}$. We averaged results over 5 experiments, and plot the outcome with one-standard-deviation error bars in Figure 8c. The semi-implicit method appears to be a clear winner.

We confirm our ability to solve large scale problems by solving problem D with $m = 10$, $K = 10$, $n = 5 \cdot 10^5$, in 10 dimensions, using the semi-implicit method, for $p = 3, 5$ and 10. This experiment is an exact replica of the timing experiment we performed with Newton’s method (for the variational formulation), in Section 3.3.4. We plot the result, averaged over 5 trials in Figure 8d.

6. EXPERIMENTS WITH REAL DATA

We report on the performance of our algorithms for real data sets. In Section 6.1 we discuss a regression problem on electric power emittance from [26, 44], while Sections 6.2 and 6.3 discuss our performance for two classification problems; the well-known MNIST (handwritten digit classification) and the more complex Fashion MNIST.

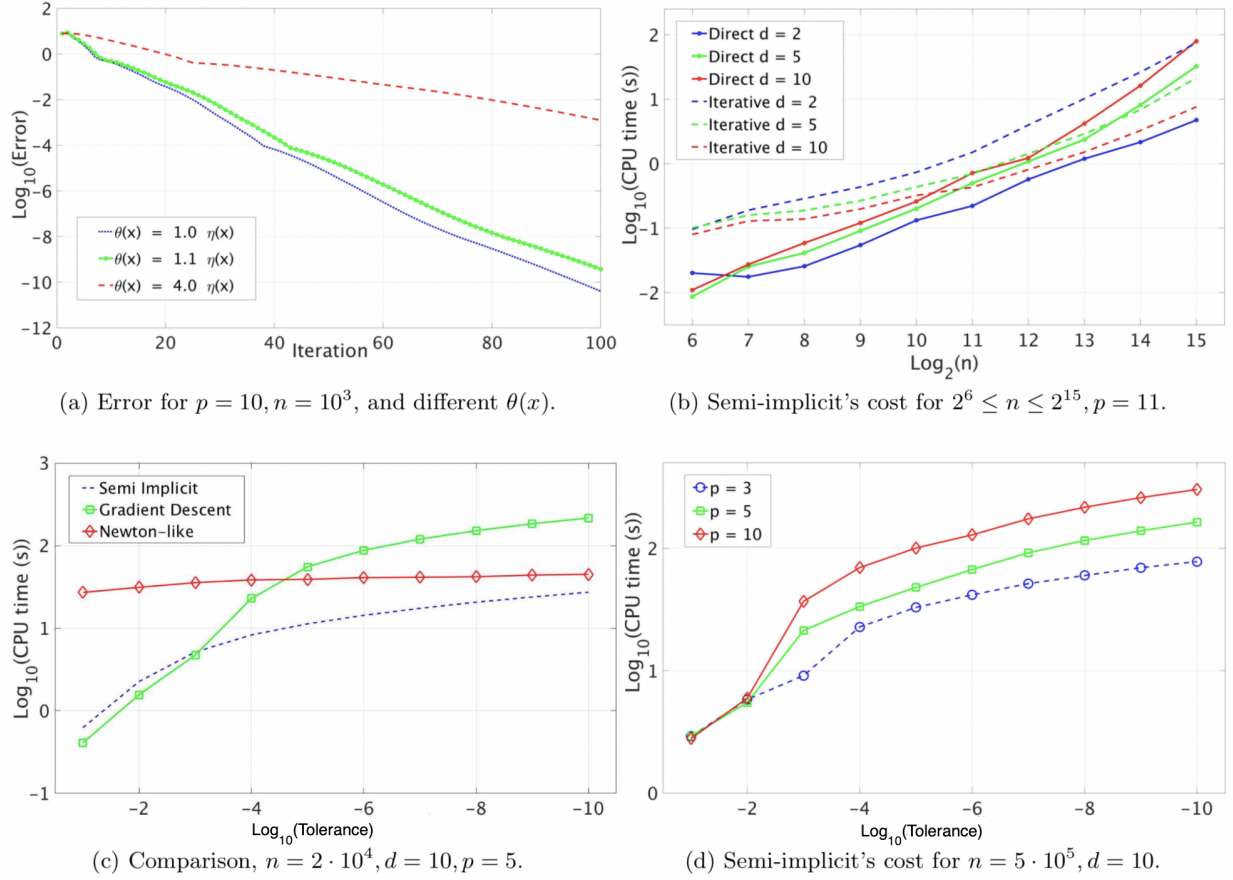


FIGURE 8. Demonstration of the competitive performance of the semi-implicit method. (a) We solve problem A with the semi-implicit method with $n = 10^3, p = 10$, and compare different choices for $\theta(x)$; smaller $\theta(x)$ (above $\eta(x)$) results in faster convergence. (b) We measure semi-implicit's cost in solving problem D, until $\epsilon < 10^{-7}$, and compare preconditioned CG with MATLAB's backslash solver, with $p = 11, m = 10$. (c) We compare the three methods on problem D with $m = 10, n = 2 \cdot 10^4, d = 10, p = 5$, and plot the amount of time required to achieve a given tolerance. Newton-like starts from $p = 2$ before solving $p = 5$. (d) We measure semi-implicit's cost in reaching a given tolerance, using preconditioned CG, for problem D, with $m = 10, d = 10, n = 5 \cdot 10^5$, and $p = 3, 5, 10$.

6.1. Power Emittance. The authors of [26, 44] considered the problem of predicting the full load electrical power output of a power plant, based on four predictors: the ambient temperature, atmospheric pressure, relative humidity and exhaust steam pressure. Such predictions can allow for the optimization of power usage. A total of 9568 observations, for the input and output variables, were collected over a period of 6 years. The authors of [44] considered a variety of machine learning algorithms, and explored feature selection exhaustively. Their best performing algorithm yield an RMSE of 3.787, which is 0.8% of the mean output variable size.

In our case, we treated this regression problem as a semi-supervised learning problem, with a number of labels $m = 10, 20, 40$ labels, and then attempted to reconstruct the output variable for the remaining $9568 - m$ points. The m labels were evenly sampled from a sorted output variable, to ensure the output domain is well represented in spite of using very few labels.

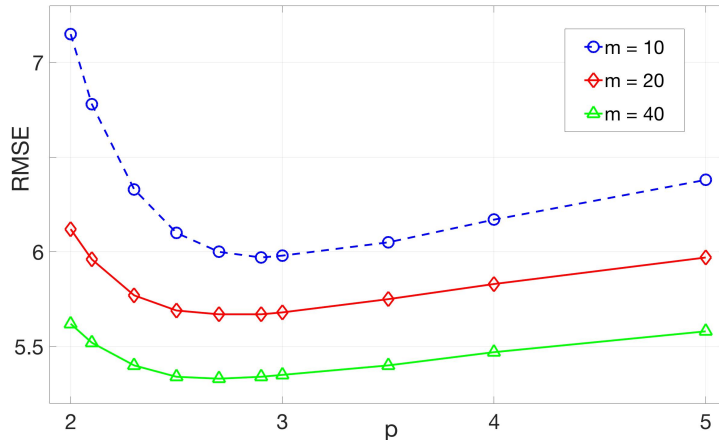


FIGURE 9. Regression results for the power emittance problem. We solve an electric power emittance regression problem, with fixed $m = 10, 20, 40$ and varying p using Newton’s method for the variational formulation, and report the RMSE.

In Figure 9, we report the RMSE we obtained when solving this problem using the variational formulation with $K = 25$ neighbors (before symmetrizing), and a variety of p values. The solution was produced using Newton’s method with homotopy. Our results illustrate the importance of using $p > 2$; in fact, $p = 3$ appears to be a near-optimal parameter. Even for $m = 10$, we are able to obtain an RMSE of 5.975 when $p = 3$, which is 1.3% of the mean output variable size. This result illustrates the effectiveness of our algorithm in producing a useful regression result in spite of using very few labeled points. As the number of labels increases, the RMSE appears to approach the RMSE reported in [44]. In fact, repeating this experiment with $m = 5000$ yields an RMSE of 4.0 when $p = 2$, though it should be noted that the Laplacian regularization formulation is not intended to be an optimal regressor when m is very large.

We also solved this problem, with the same parameters, using the game theoretic formulation, and obtained a very similar regression quality. In fact, $p = 3$ once again appears to be an optimal parameter, and the similarity of the results supports the notion that the variational and game theoretic formulations are equally useful for learning problems.

6.2. MNIST digit classification. The well-known MNIST dataset of handwritten digits is a standard benchmark for machine learning algorithms, and has been used to report the performance of a variety of algorithms, in hundreds of publications, since [28]. The dataset consists of 70,000 handwritten digits, 60,000 for training, and 10,000 for testing. Each image is represented in 28×28 pixels in grayscale, meaning it can be represented as a vector of 784 dimensions, and corresponds to a 0–9 digit. See Figure 10 for a sample of these handwritten digits. The classes are well balanced, meaning there are roughly 7,000 examples of each digit.

Rather than solving the standard classification problem (using 60,000 training images to learn how to classify the remaining 10,000), we consider the significantly more challenging task of treating this problem as a semi-supervised problem, with very few labels, and attempt to classify the rest.

We solve this multi-class classification problem by solving 10 binary classification problems, one for each digit. At each iteration, we choose just one digit, say 3, and then assign a score to every other image, depending on how similar they are to 3. A high score means the digit is likely to be a 3, a low score means the digit is unlikely to be a 3. Each image gets assigned a similarity score to each digit. At the end, each image is labeled by the digit that produced the largest score.



FIGURE 10. Sample handwritten digits from the MNIST dataset.

The authors of [42] attempted to solve this problem with a graph-based approach, by re-weighting the graph more heavily near neighbors, but their formulation was shown to be ill-posed in [8], which also proposed a new and well-posed formulation to solve this problem. We will compare our results against the results obtained using both formulations. Similar to both papers, we shall report performance for $m = 10, 30, 50, 70, 100$, where $m = 10$ means we are only providing one labeled example for each digit. We precomputed 100 permutations of the dataset, to determine which images get labeled, and used the same permutations across all experiments for consistency.

Figure 11a reports the performance of 5 formulations: the standard 2-Laplacian [54], the ∞ -Laplacian (also known as Lipschitz learning), the variational formulation of the p -Laplacian with $p = 4$, the game-theoretic formulation of the p -Laplacian with $p = 5$, and the weighted Laplacian [42]. We also computed results for the Properly Weighted Laplacian [8], but they are very similar to the weighted Laplacian, so we do not report them. The variational result was produced using Newton’s method, while the Lipschitz learning problem, and the game theoretic formulation were solved using the semi-implicit method. The resulting linear systems were solved with indirect methods (for speed), but using a direct solver in many test cases produced the same results. Stopping tolerances of $\epsilon < 10^{-8}$ (for Newton) and $\epsilon < 10^{-3}$ (for semi-implicit method) produce consistent results.

Although we only report our results with $K = 10$, we also performed all experiments with $K = 25$ and $K = 50$, and consistently found that increasing the number of neighbors in the graph does not provide any advantages. In fact, it often decreases accuracy, while increasing the cost substantially. These results support our belief that the graph should have just enough edges to be connected.

All formulations improve their accuracy and consistency as the number of labels increases, reaching a similar level when $m = 100$. The best way to observe the difference between these methods is to see the classification accuracy when the number of labels is small. In particular, when $m = 10$ one can really see the superiority of the p -Laplacian model (both variational and game-theoretic) over the 2-Laplacian. Our results also outperform the Weighted Laplacian while in this case also providing much more consistent results. Indeed, the standard deviations of our method were smaller, but we did not report them here.

In order to provide further evidence of the superiority of the p -Laplacian model, we fixed $m = 10$, and $K = 10$, and decrease the number of unlabeled images. The premise of a semi-supervised learning model is that we may achieve superior performance by including both labeled and unlabeled data. If we keep m fixed, we should expect the accuracy to improve as the number of unlabeled images increases. For this experiment, we reduced the number of images from 70,000 down to 2188, and produced 100 permutations for the labeled images, which were used across all experiments for consistency. We report the results of this experiment in Figure 11b, for the 2-Laplacian, the p -Laplacian (game-theoretic formulation), with $p = 3, 4, 5$, as well as the Weighted Laplacian model. The results provide strong evidence that the 2-Laplacian is an ill-posed formulation, since accuracy drops dramatically, from 49.6% with 2188 images, down to just 15% with 70,000 images. The Weighted Laplacian also deteriorates with an increase in the number of images (more slowly), while the p -Laplacian, for $p = 5$ improves gradually as the amount of unlabeled data increases.

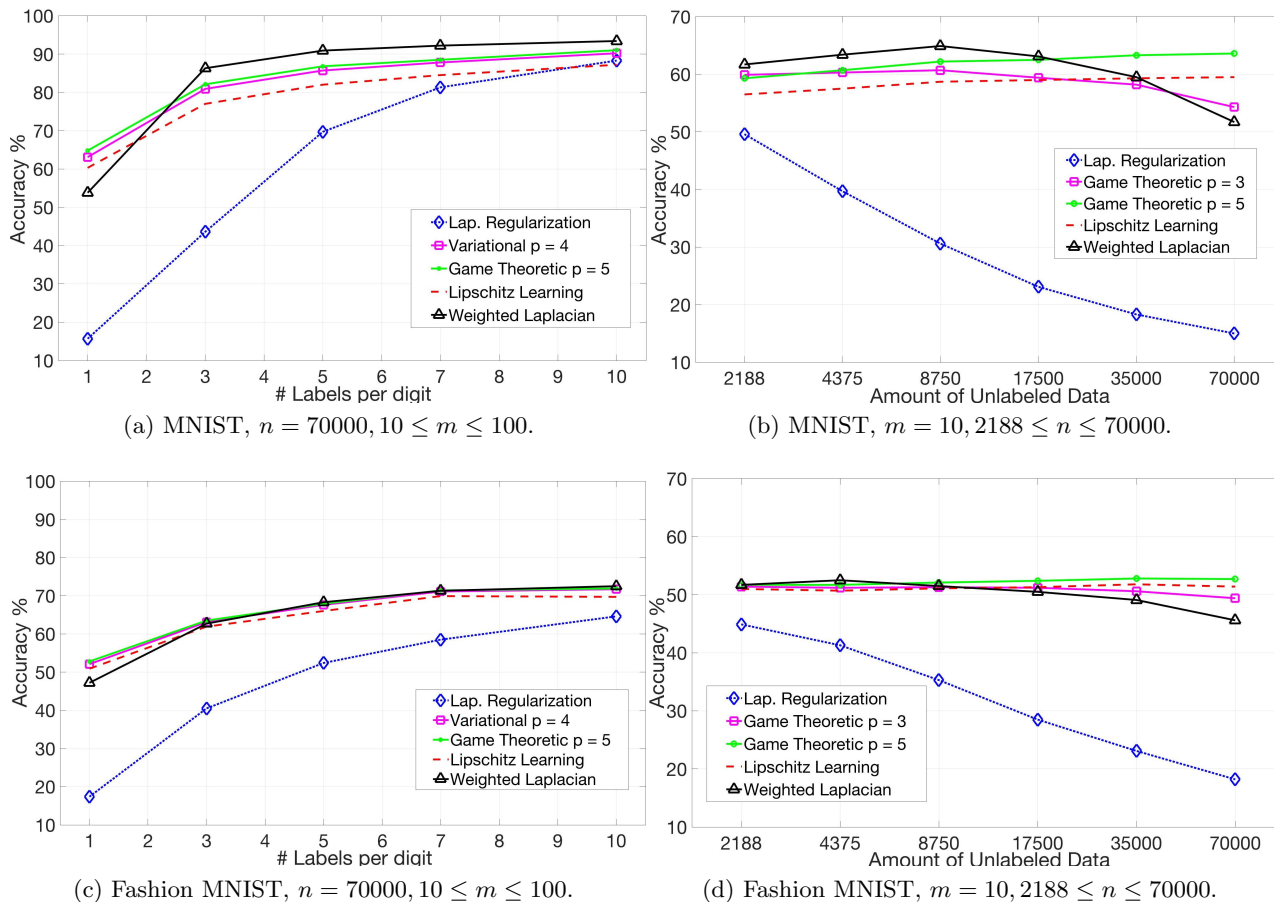


FIGURE 11. Classification accuracy for the MNIST and Fashion MNIST datasets. (a) Classification accuracy for MNIST, averaged over 50 experiments. (b) Classification accuracy for MNIST with $m = 10$ and varying size n , averaged over 100 experiments, of sampled unlabeled data. Plots in (c) and (d) are analogous to those in (a) and (b) for Fashion MNIST.



FIGURE 12. Sample 28×28 -pixel images from the Fashion MNIST dataset.

6.3. Fashion MNIST. The dataset Fashion MNIST, recently introduced by [47] was designed as a drop-in replacement for MNIST, in order to test classification accuracy for a significantly harder problem. This dataset also consists of 60,000 training images, and 10,000 testing images, of size 28×28 pixels, in grayscale. Handwritten digits are replaced by 10 classes of clothing items, such as sandals, and dresses, derived from Zalando’s online catalog. For an example, see Figure 12.

We repeated our MNIST experiment for this dataset, using identical parameters and solvers, and report the results in Figure 11c and 11d. Classification performance is lower, as expected, given the increasing difficulty of the problem. The p -Laplace formulation (both variational and game-theoretic) still outperform the 2-Laplacian by a large margin, and seem to outperform other formulations, in the regime of few labels and large unlabeled sample, by a small margin in accuracy, while also providing much more consistent results.

Finally, we mention that for both the MNIST and Fashion MNIST experiments, we are simply using the Euclidean distance between images to define the weights in the graph. Better results can be obtained for all algorithms by using an image metric based on a feature transformation, such as the Scale Invariant Feature Transformation (SIFT) [32], or the scattering transformation [2], among others. Our goal in this paper is to develop algorithms for the graph p -Laplacian learning problem and examine the role of the parameter p . As such, improvements in the construction of the graph are outside the scope of the paper.

7. CONCLUSIONS

In this paper we studied and developed algorithms for solving the variational and game-theoretic formulations of the p -Laplacian in a graph. The variational formulation may be solved efficiently using Newton’s method with homotopy, while the semi-implicit method is the fastest and most reliable approach for solving the game-theoretic formulation. Our experiments with real data seem to suggest that both formulations are equally good for semi-supervised learning tasks, which provides additional flexibility in choosing a suitable method.

REFERENCES

- [1] M. Alamgir and U. V. Luxburg. Phase transition in the family of p -resistances. In *Advances in Neural Information Processing Systems*, pages 379–387, 2011.
- [2] J. Andén and S. Mallat. Deep scattering spectrum. *IEEE Transactions on Signal Processing*, 62(16):4114–4128, 2014.
- [3] R. K. Ando and T. Zhang. Learning on graph with Laplacian regularization. In *Advances in neural information processing systems*, pages 25–32, 2007.
- [4] G. Aronsson, M. Crandall, and P. Juutinen. A tour of the theory of absolutely minimizing functions. *Bulletin of the American mathematical society*, 41(4):439–505, 2004.
- [5] N. Bridle and X. Zhu. p -voltages: Laplacian regularization for semi-supervised learning on high-dimensional data. In *Eleventh Workshop on Mining and Learning with Graphs (MLG2013)*, 2013.
- [6] J. Calder. Consistency of Lipschitz learning with infinite unlabeled data and finite labeled data. *arXiv:1710.10364*, 2017.
- [7] J. Calder. The game theoretic p -Laplacian and semi-supervised learning with few labels. *To appear in Nonlinearity*, 2018.
- [8] J. Calder and D. Slepcev. Properly-weighted graph Laplacian for semi-supervised learning. *arXiv:1810.04351*, 2018.
- [9] J. Calder and A. Yezzi. PDE acceleration: A convergence rate analysis and applications to obstacle problems. *arXiv:1810.01066*, 2018.
- [10] A. Chambolle and T. Pock. A first-order primal-dual algorithm for convex problems with applications to imaging. *Journal of mathematical imaging and vision*, 40(1):120–145, 2011.
- [11] T. F. Chan and P. Mulet. On the convergence of the lagged diffusivity fixed point method in total variation image restoration. *SIAM journal on numerical analysis*, 36(2):354–367, 1999.
- [12] O. Chapelle, B. Scholkopf, and A. Zien. *Semi-supervised learning*. MIT, 2006.
- [13] T. A. Davis. Algorithm 832: Umfpack v4. 3—an unsymmetric-pattern multifrontal method. *ACM Transactions on Mathematical Software (TOMS)*, 30(2):196–199, 2004.
- [14] I. S. Duff. Ma57—a code for the solution of sparse symmetric definite and indefinite systems. *ACM Transactions on Mathematical Software (TOMS)*, 30(2):118–144, 2004.
- [15] A. El Alaoui, X. Cheng, A. Ramdas, M. J. Wainwright, and M. I. Jordan. Asymptotic behavior of ℓ_p -based Laplacian regularization in semi-supervised learning. In *Conference on Learning Theory*, pages 879–906, 2016.
- [16] A. Elmoataz, X. Desquesnes, and M. Toutain. On the game p -Laplacian on weighted graphs with applications in image processing and data clustering. *European Journal of Applied Mathematics*, 28(6):922–948, 2017.

- [17] A. Elmoataz, F. Lozes, and M. Toutain. Nonlocal PDEs on graphs: From tug-of-war games to unified interpolation on images and point clouds. *Journal of Mathematical Imaging and Vision*, 57(3):381–401, 2017.
- [18] A. Elmoataz, M. Toutain, and D. Tenbrinck. On the p -Laplacian and ∞ -Laplacian on graphs with applications in image and data processing. *SIAM Journal on Imaging Sciences*, 8(4):2412–2451, 2015.
- [19] L. Evans. *Partial Differential Equations (Graduate Studies in Mathematics, V. 19) GSM/19*. American Mathematical Society, June 1998.
- [20] R. Fletcher, J. Grant, and M. Hebden. The calculation of linear best L_p approximations. *The Computer Journal*, 14(3):276–279, 1971.
- [21] B. D. Froese and A. M. Oberman. Convergent finite difference solvers for viscosity solutions of the elliptic monge–ampère equation in dimensions two and higher. *SIAM Journal on Numerical Analysis*, 49(4):1692–1714, 2011.
- [22] Y. Hafiene, J. Fadili, and A. Elmoataz. Nonlocal p -Laplacian variational problems on graphs. *arXiv:1810.12817*, 2018.
- [23] J. He, M. Li, H.-J. Zhang, H. Tong, and C. Zhang. Manifold-ranking based image retrieval. In *Proceedings of the 12th annual ACM international conference on Multimedia*, pages 9–16. ACM, 2004.
- [24] J. He, M. Li, H.-J. Zhang, H. Tong, and C. Zhang. Generalized manifold-ranking-based image retrieval. *IEEE Transactions on image processing*, 15(10):3170–3177, 2006.
- [25] N. J. Higham. *Analysis of the Cholesky decomposition of a semi-definite matrix*. Oxford University Press, 1990.
- [26] H. Kaya, P. Tüfekci, and F. S. Gürgen. Local and global learning methods for predicting power of a combined gas & steam turbine. In *Proceedings of the International Conference on Emerging Trends in Computer and Electronics Engineering ICETCEE*, pages 13–18, 2012.
- [27] R. Kyng, A. Rao, S. Sachdeva, and D. A. Spielman. Algorithms for Lipschitz learning on graphs. In *Conference on Learning Theory*, pages 1190–1223, 2015.
- [28] Y. LeCun, L. Bottou, Y. Bengio, and P. Haffner. Gradient-based learning applied to document recognition. *Proceedings of the IEEE*, 86(11):2278–2324, 1998.
- [29] G. Leoni. *A first course in Sobolev spaces*. American Mathematical Soc., 2017.
- [30] M. Lewicka and J. J. Manfredi. Game theoretical methods in PDEs. *Bollettino dell’Unione Matematica Italiana*, 7(3):211–216, 2014.
- [31] P. Lindqvist. *Notes on the p -Laplace equation*. 2017.
- [32] D. G. Lowe. Object recognition from local scale-invariant features. In *Computer vision, 1999. The proceedings of the seventh IEEE international conference on*, volume 2, pages 1150–1157. Ieee, 1999.
- [33] U. v. Luxburg and O. Bousquet. Distance-based classification with Lipschitz functions. *Journal of Machine Learning Research*, 5(Jun):669–695, 2004.
- [34] J. J. Manfredi, A. M. Oberman, and A. P. Sviridov. Nonlinear elliptic partial differential equations and p -harmonic functions on graphs. *Differential Integral Equations*, 28(1-2):79–102, 2015.
- [35] B. Nadler, N. Srebro, and X. Zhou. Semi-supervised learning with the graph Laplacian: The limit of infinite unlabelled data. *Advances in neural information processing systems*, 22:1330–1338, 2009.
- [36] A. M. Oberman. Finite difference methods for the infinity laplace and p -laplace equations. *Journal of Computational and Applied Mathematics*, 254:65–80, 2013.
- [37] J. M. Ortega. The newton-kantorovich theorem. *The American Mathematical Monthly*, 75(6):658–660, 1968.
- [38] Y. Peres, O. Schramm, S. Sheffield, and D. Wilson. Tug-of-war and the infinity Laplacian. *Journal of the American Mathematical Society*, 22(1):167–210, 2009.
- [39] T. Pock, D. Cremers, H. Bischof, and A. Chambolle. An algorithm for minimizing the mumford-shah functional. In *Computer Vision, 2009 IEEE 12th International Conference on*, pages 1133–1140. IEEE, 2009.
- [40] R. T. Rockafellar. *Convex analysis*. Princeton university press, 2015.
- [41] Y. Saad and M. H. Schultz. Gmres: A generalized minimal residual algorithm for solving nonsymmetric linear systems. *SIAM Journal on scientific and statistical computing*, 7(3):856–869, 1986.
- [42] Z. Shi, S. Osher, and W. Zhu. Weighted nonlocal Laplacian on interpolation from sparse data. *Journal of Scientific Computing*, 73(2-3):1164–1177, 2017.
- [43] D. Slepcev and M. Thorpe. Analysis of p -Laplacian regularization in semi-supervised learning. *arXiv:1707.06213*, 2017.
- [44] P. Tüfekci. Prediction of full load electrical power output of a base load operated combined cycle power plant using machine learning methods. *International Journal of Electrical Power & Energy Systems*, 60:126–140, 2014.
- [45] R. A. Vargas and C. S. Burrus. Iterative design of lp fir and iir digital filters. In *2009 IEEE 13th Digital Signal Processing Workshop and 5th IEEE Signal Processing Education Workshop*, pages 468–473, Jan 2009.
- [46] Y. Wang, M. A. Cheema, X. Lin, and Q. Zhang. Multi-manifold ranking: Using multiple features for better image retrieval. In *Pacific-Asia Conference on Knowledge Discovery and Data Mining*, pages 449–460. Springer, 2013.

- [47] H. Xiao, K. Rasul, and R. Vollgraf. Fashion-mnist: a novel image dataset for benchmarking machine learning algorithms. *arXiv:1708.07747*, 2017.
- [48] B. Xu, J. Bu, C. Chen, D. Cai, X. He, W. Liu, and J. Luo. Efficient manifold ranking for image retrieval. In *Proceedings of the 34th international ACM SIGIR conference on Research and development in Information Retrieval*, pages 525–534. ACM, 2011.
- [49] C. Yang, L. Zhang, H. Lu, X. Ruan, and M.-H. Yang. Saliency detection via graph-based manifold ranking. In *Proceedings of the IEEE conference on computer vision and pattern recognition*, pages 3166–3173, 2013.
- [50] D. Zhou, O. Bousquet, T. N. Lal, J. Weston, and B. Schölkopf. Learning with local and global consistency. In *Advances in neural information processing systems*, pages 321–328, 2004.
- [51] D. Zhou, J. Huang, and B. Schölkopf. Learning from labeled and unlabeled data on a directed graph. In *Proceedings of the 22nd international conference on Machine learning*, pages 1036–1043. ACM, 2005.
- [52] D. Zhou and B. Schölkopf. Regularization on discrete spaces. In *Joint Pattern Recognition Symposium*, pages 361–368. Springer, 2005.
- [53] D. Zhou, J. Weston, A. Gretton, O. Bousquet, and B. Schölkopf. Ranking on data manifolds. In *Advances in neural information processing systems*, pages 169–176, 2004.
- [54] X. Zhu, Z. Ghahramani, and J. D. Lafferty. Semi-supervised learning using gaussian fields and harmonic functions. In *Proceedings of the 20th International conference on Machine learning (ICML-03)*, pages 912–919, 2003.
- [55] D. Zosso, B. Osting, M. M. Xia, and S. J. Osher. An efficient primal-dual method for the obstacle problem. *Journal of Scientific Computing*, 73(1):416–437, 2017.

APPENDIX A. DETAILS ON PRIMAL DUAL FORMULATION

Here, we present the proofs of some results used in Section 2.3 in developing the primal dual formulation.

A.1. Derivation of graph divergence. Recall the graph divergence is defined by the identity

$$(\nabla u, v)_{L^2(E)} = (-\operatorname{div}(v), u)_{L^2(\mathcal{X})}.$$

To obtain an expression for $\operatorname{div}(v)$ we compute

$$\begin{aligned} (\nabla u, v)_{L^2(E)} &= \sum_{(x,y) \in E} (u(x) - u(y))v(x, y) \\ &= \sum_{(x,y) \in E} u(x)v(x, y) - \sum_{(x,y) \in E} u(x)v(y, x) \\ &= \sum_{(x,y) \in E} u(x)(v(x, y) - v(y, x)) \\ &= - \sum_{x \in \mathcal{X}} \left(\sum_{y \sim x} [v(y, x) - v(x, y)] \right) u(x), \end{aligned}$$

and therefore, we have

$$\operatorname{div}(v)(x) = \sum_{y \sim x} v(y, x) - v(x, y).$$

If v is skew-symmetric, so that $v(x, y) = -v(y, x)$, then

$$\operatorname{div}(v)(x) = -2 \sum_{y \sim x} v(x, y).$$

A.2. Legendre-Fenchel transform. Here, we compute the Legendre-Fenchel transform of J_p , defined in (2.10). By definition we have

$$J_p^*(u, v) = \max_{z \in L^2(E)} \left\{ \sum_{(x,y) \in E} v(x, y)z(x, y) - \frac{1}{2p} \sum_{(x,y) \in E} w_{xy} |z(x, y)|^p - \sum_{x \in \mathcal{X}} f(x)u(x) \right\}.$$

A maximizer $z(x, y)$ satisfies the optimality condition

$$(A.1) \quad v(x, y) - \frac{1}{2}w_{xy}|z(x, y)|^{p-2}z(x, y) = 0.$$

Therefore, we have

$$|v(x, y)| = \frac{1}{2}w_{xy}|z(x, y)|^{p-1} \quad \text{and} \quad \text{sign}(v) = \text{sign}(z),$$

and so

$$|z(x, y)|^p = 2^q w_{xy}^{-q} |v(x, y)|^q,$$

where $\frac{1}{p} + \frac{1}{q} = 1$. It follows that

$$v(x, y)z(x, y) = 2^{q-1}w_{x,y}^{1-q}|v(x, y)|^q,$$

which yields

$$\begin{aligned} J_p^*(u, v) &= \sum_{(x,y) \in E} 2^{q-1}w_{xy}^{1-q}|v(x, y)|^q - \frac{1}{p} \sum_{(x,y) \in E} 2^{q-1}w_{xy}^{1-q}|v(x, y)|^q - \sum_{x \in \mathcal{X}} f(x)u(x) \\ &= \frac{2^q}{2q} \sum_{(x,y) \in E} w_{xy}^{1-q}|v(x, y)|^q - \sum_{x \in \mathcal{X}} f(x)u(x). \end{aligned}$$

A.3. Skew-symmetry in dual problem. We show here that the dual problem (2.17) preserves skew-symmetry. That is, if $v^k(x, y) = -v^k(y, x)$ then $v^{k+1}(x, y) = -v^{k+1}(y, x)$, for all $(x, y) \in E$. To see this, assume $v^k(x, y) = -v^k(y, x)$. By differentiating (2.17) we see that

$$\bar{u}^k(x) - \bar{u}^k(y) = 2^{q-1}w_{xy}^{1-q}|v^{k+1}(x, y)|^{q-2}v^{k+1}(x, y) + \frac{1}{r_1}(v^{k+1}(x, y) - v^k(x, y)),$$

and

$$\bar{u}^k(x) - \bar{u}^k(y) = 2^{q-1}w_{xy}^{1-q}|-v^{k+1}(y, x)|^{q-2}(-v^{k+1}(y, x)) + \frac{1}{r_1}(-v^{k+1}(y, x) - v^k(x, y)),$$

where we used the skew-symmetry of v^k in the second equation. Since minimizers of (2.17) are unique (by strict convexity), we have $v^{k+1}(x, y) = -v^{k+1}(y, x)$.

A.4. Solving the dual problem . We describe here how to solve the dual problem (2.17), which is equivalent to the one dimensional minimization problem

$$(A.2) \quad \min_{\nu \in \mathbb{R}} \left\{ a\nu + \frac{1}{2r}(\nu - b)^2 + \frac{c}{q}|\nu|^q \right\},$$

where $c > 0, q \geq 1$. By completing the square, we can equivalently solve the problem

$$\min_{\nu \in \mathbb{R}} \{(\nu - \alpha)^2 + \beta|\nu|^q\}.$$

where $\alpha = b - ar$ and $\beta = 2cr/q > 0$. The resulting optimality condition is

$$G(\nu, \alpha, \beta, q) := 2\nu - 2\alpha + \beta|\nu|^{q-2}\nu = 0.$$

From this, we obtain $\text{sign}(\nu) = \text{sign}(\alpha)$, and so $\nu = \mu \text{sign}(\alpha)$, where $\mu \geq 0$ is the solution of

$$G(\mu, |\alpha|, \beta, q) = 0.$$

Since $\mu \mapsto G(\mu, |\alpha|, \beta, q)$ is strictly increasing, the solution can be computed with a bisection search on the interval $\mu \in [0, |\alpha|]$. It is also possible to use Newton's method, however, when q is close to $q = 1$, the number of steps required can exceed the number of bisection steps.